ACS OMEGA

Open Access

http://pubs.acs.org/journal/acsodf

Article

Design, Characterization, Antimicrobial Activity, and *In Silico* Studies of Theinothiazoloquinazoline Derivatives Bearing Thiazinone, Tetrazole, and Triazole Moieties

Hagar S. El-Hema,* Sara. M. Soliman, Wagdy El-Dougdoug, Mohamed H. M. Ahmed, Abdelmotaal Abdelmajeid, Eman S. Nossier, Modather F. Hussein, Ashtar A. Alrayes, Mariam Hassan, Noha A. Ahmed, Amr Sabry, and Adel A.-H. Abdel-Rahman*

Cite This: *ACS Omega* 2025, 10, 9703−9717

Read Online

ACCESS | Metrics & More | Article Recommendations | Supporting Information

ABSTRACT: The pressing demand for novel antibiotics to counter drug-resistant bacteria, such as methicillin-resistant *Staphylococcus aureus* (MRSA), underscores the serious public health threat posed by antibiotic resistance. To address this issue, novel quinazoline-4-one derivatives were developed, synthesized, and evaluated *in vitro* against a range of pathogens, including fungi like *Aspergillus fumigatus* (RCMB 002008), Gram-negative bacteria like *Escherichia coli* (ATCC 25922), and Gram-positive bacteria like *Staphylococcus aureus* (ATCC 25923) and MRSA (USA300). Notably, the thieno-thiazolo-quinazoline compounds **4** and **5** demonstrated a strong ability to inhibit and disrupt MRSA USA300 biofilm formation across all tested concentrations. Furthermore, in an *in vivo* MRSA skin infection model, these compounds effectively reduced bacterial counts compared to both vehicle-treated and untreated control groups. To enhance understanding and provide deeper insights, ADMET and docking simulations were also conducted.

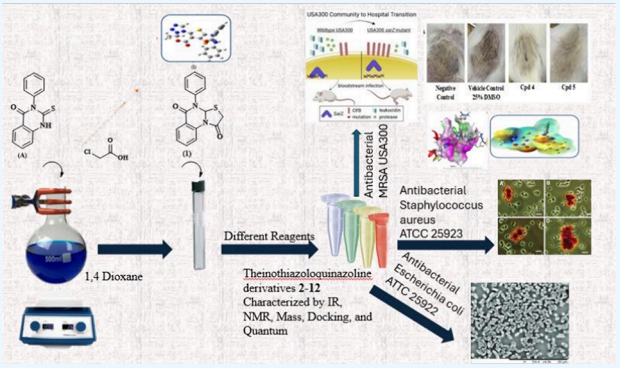

1. INTRODUCTION

According to WHO predictions, antibiotic-resistant strains will kill 10 million people globally each year by 2050, surpassing the death toll from AIDS, cancer, and having a significant effect on the world economy.[1,2] The stock of effective antibiotics quickly decreases as microbes evolve new resistance mechanisms, posing considerable difficulties to current treatment methods.[3,4] The ESCAPE pathogens—*Enterococcus faecium, Staphylococcus aureus, Clostridium difficile, Acinetobacter baumannii, Pseudomonas aeruginosa,* and *Enterobacter* species—present a significant challenge in healthcare settings due to their high resistance to multiple drugs.[5]

Methicillin-resistant *Staphylococcus aureus* (MRSA) exhibits this problem since it routinely develops resistance to new medications. This resistance complicates treatment options while also imposing a significant fiscal burden on global healthcare systems.[6−8] MRSA resistance strategies include changes in target locations, the development of antibiotic-inactivating enzymes, and adjustments to cell membrane permeability, among others. This growing resistance emphasizes the critical need for pharmaceutical innovation to discover and develop novel medicines capable of battling these hardy pathogens.[9]

Among various antibacterial targets, bacterial type II topoisomerases, including DNA gyrase, have been recognized as crucial therapeutic targets for antibacterial agents.[10] These heterotetrametric enzymes are made up of two GyrA and two GyrB subunits (A2B2). In order to prevent positive supercoiling from overtwisting DNA and shattering DNA strands and to preserve equilibrium in bacterial DNA replication, DNA gyrase plays a unique role in negative supercoiling. GyrB provides energy for the enzyme's catalytic function through ATP hydrolysis, whereas GyrA is mainly engaged in the breaking and reunification of double-stranded DNA.[11,12] Therefore, DNA gyrase will remain crucial for bacterial survival.[13]

Quinazoline and Quinazolinone derivatives were considered as a source of useful pharmacophores for novel drug evolution and still gain enormous attention nowadays[14,15] Due to multiple substitutions on this ring system. Moreover, the

Received: December 10, 2024
Revised: February 7, 2025
Accepted: February 12, 2025
Published: February 28, 2025

broad variety of therapeutic properties of quinazolinones have drawn much attention and great application in drug discovery.[16] such as sedative,[17] hypoglycemic,[18] anticonvulsant,[19,20] herbicidal,[21] antibacterial,[22,23] antifungal,[24] antileishmanial,[25] antioxidant,[26] antioxidant,[27] diuretic activities,[28] anti-inflammatory,[29,30] cytotoxicity,[31,32] antitumor,[33,34] anti-HIV,[35] antiviral,[32] antituberculosis[31] properties, in addition to their inhibitory effects on tyrosine kinase,[36−38] thymidylate synthase[37,39] and poly(ADP-ribose) polymerase (PARP),[17] and other plentiful uses and interesting properties. These examples highlight their widespread presence in bioorganic and medicinal chemistry. In this article, we focus on quinazolinones and their various derivatives with antimicrobial activity.[40−43]

In searching for novel medications, particularly those related to antibacterial drugs, heterocycles are essential structural motifs.[44,45] Incorporating heteroatoms into the cyclic structures of these compounds enhances their interactions with various biological macromolecules, such as DNA, proteins, and enzymes, significantly boosting their biological activity.[46,47] Various compounds **I-VI** in (Figure 1), either with

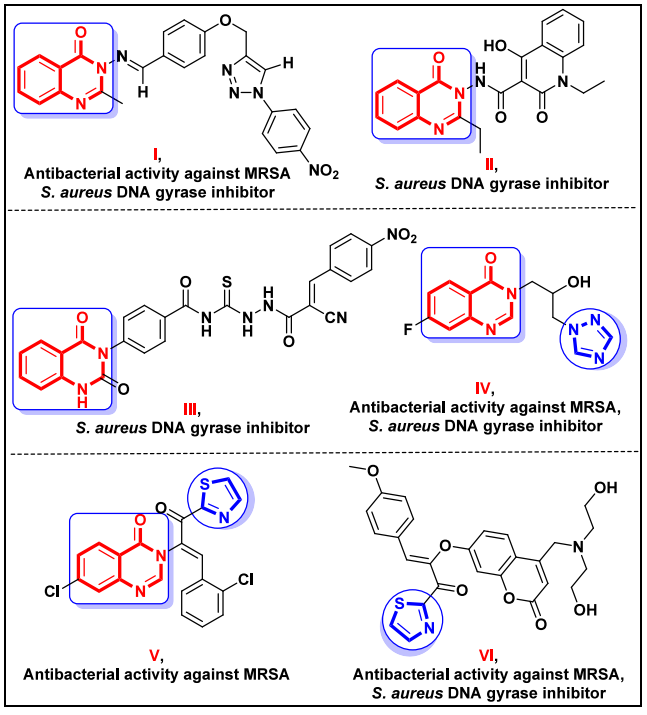

Figure 1. Various antimicrobial agents, bearing quinazolinone and other nitrogenous moieties as, thiazole, or triazole constituents, with *Staphylococcus aureus* DNA gyrase inhibition mechanism.

quinazolinone and/or with other nitrogenous moieties such as thiazole or triazole, were shown to have significant antimicrobial activity, including against MRSA.[48−53] Additionally, their antimicrobial potency was furnished through inhibition of *Staphylococcus aureus* DNA gyrase.

Building on the broad medicinal potential of quinazoline-4-one and inspired by the structural characteristics of compound I, new quinazoline-4-one derivatives were strategically designed and synthesized. This was achieved through molecular hybridization with other pharmacophoric groups, aiming to enhance their biological activity (Figure 2). All derivatives were screened *in vitro* for their antimicrobial activities versus *Staphylococcus aureus* (ATCC 25923) and methicillin-resistant

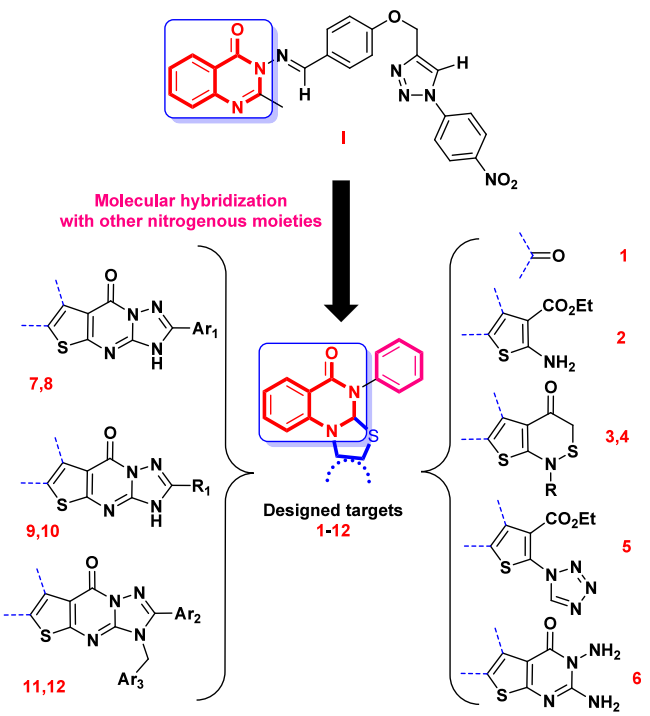

Figure 2. Designed rationale for quinazolinone-based derivatives **1**−**12** fused with various nitrogenous moieties as antimicrobial agents targeting inhibition of *Staphylococcus aureus* DNA gyrase.

Staphylococcus aureus (*MRSA*, USA300) as Gram-positive bacterial examples, *Escherichia coli* (ATCC 25922) as a Gram-negative bacterial example, and *Aspergillus fumigatus* (RCMB 002008) as a fungal example. The promising compounds were further subjected to *in vitro* antibiofilm activity and an *in vivo* MRSA skin infection model. Moreover, *in silico* ADMET assessment and docking simulation were applied to describe their pharmacokinetic characteristics along with their potential as crucial antimicrobial candidates.

2. RESULTS AND DISCUSSION

2.1. Chemistry. The synthetic methods used to produce the intermediate and final compounds are outlined in Schemes 1−5, respectively. In Scheme 1, the desired 4-Phenyl-3a,4-dihydro-5*H*-thiazolo[3,2-*a*]quinazoline-1,5(2H)-dione (**1**) was prepared with 72% yield by reacting the starting material 3-phenyl-2-thioxo-2,3-dihydroquinazolin-4(1*H*)-one[54] (**A**) with chloroacetic acid in dry 1,4 dioxane under refluxing conditions for 2 h using a Dean−Stark condenser, followed by an efficient transformation with ethyl cyanoacetate, sulfur, and diethylamine in dry DMF at 50 °C for 2 h to yield ethyl 9-amino-5-oxo-6-phenyl-6,6a-dihydro-5*H*-thieno[2′,3′:4,5]thiazolo[3,2-*a*]quinazoline-8-carboxylate (**2**). The confirmation of the final chemical structures of compounds 1 and 2 was carried out through the analysis of analytical and spectral data, while the purity of the compounds was assessed using thin-layer chromatography (TLC). For instance, in the case of compound **1**, the IR spectrum revealed absorption bands at 2936 and 1730 cm^{-1}, corresponding to the CH-aliphatic and C = O (thiazolidin-4-one) groups, respectively. Additionally, in the ^{1}H NMR spectrum, singlet signals at 4.16 and 7.22 ppm were observed, which were attributed to the thiazole protons. Moreover, the ^{13}C NMR spectrum displayed distinct signals at 45.51, 90.00, and 172.37 ppm, corresponding to the triazole

https://doi.org/10.1021/acsomega.4c11076
ACS Omega 2025, 10, 9703−9717

Scheme 1. Synthesis of Thiazolo[3,2-*a*]quinazoline-1,5-dione 1 and Ethyl 9-Amino-thieno[2′,3′:4,5]thiazolo[3,2-*a*]quinazoline-8-carboxylate 2

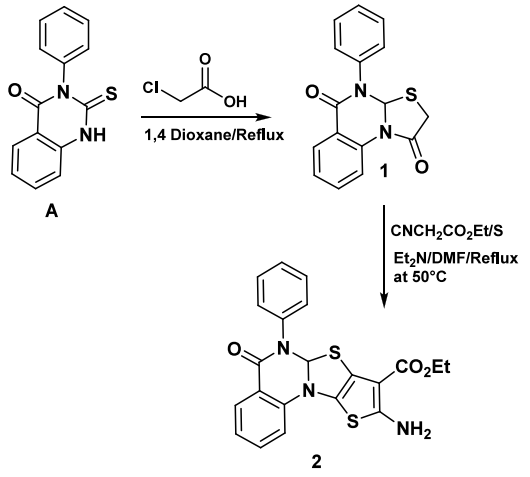

Scheme 2. Synthesis of Thieno-thiazolo-quinazoline Derivatives 3−6

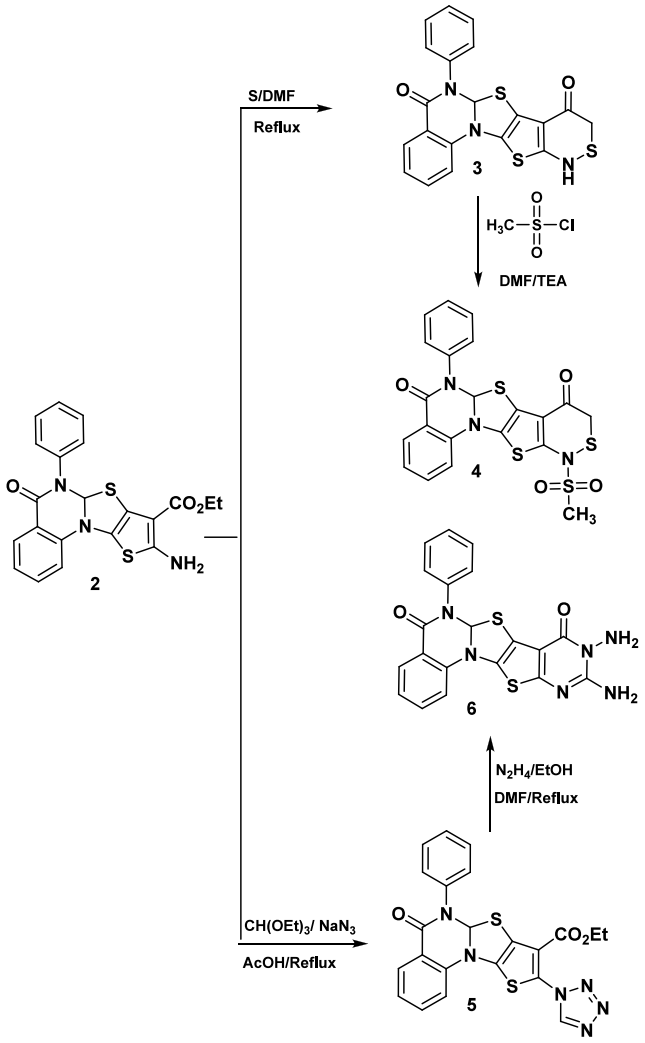

CH_2, CH, and C = O carbons, respectively. In the case of compound **2**, the IR spectrum revealed absorption bands at 3239, 3219, and 1719 cm^{-1}, corresponding to the NH_2 and C = O ester groups, respectively, and showed an absence of an absorption band at 1730 cm^{-1}, corresponding to the C = O (thiazolidin-4-one) group. Additionally, in the ^1H NMR spectrum, a triplet signal at 1.50 ppm, a quartet signal at 4.20 ppm, and a broad signal at 6.40 ppm were observed, which were attributed the ester and amino protons, respectively, and the absence of a signal at 4.16 ppm, which was attributed to the CH_2 protons. Moreover, the ^{13}C NMR spectrum displayed distinct signals at 12.34, 63.65, and 156.06 ppm, corresponding to the CH_3, CH_2, and C = O carbons, respectively, and the absence of signals at 45.51 and 172.37 ppm, corresponding to the CH_2 and C = O (thiazolidin-4-one) carbons.

In Scheme 2, the desired 1,2-thiazinan-5-one derivative (**3**) was prepared in 66% yield by reacting **2** with sulfur in dry DMF to yield 6-phenyl-6,6a-dihydro-5*H*,9*H*-[1,2]thiazino-[4″,3″:4′,5′]thieno[2′,3′:4,5]thiazolo[3,2-*a*]quinazoline-5,8-(11*H*)-dione (**3**), followed by reaction with methane sulfonyl chloride in the presence of triethylamine as a catalyst in dry DMF to yield 11-(methylsulfonyl)-6-phenyl-6,6a-dihydro-5*H*,9*H*-[1,2]thiazino[4″,3″:4′,5′]thieno[2′,3′:4,5]thiazolo[3,2-*a*]quinazoline-5,8(11H)-dione (**4**). The confirmation of the final chemical structures of compounds **3** and **4** was achieved through the analysis of both analytical and spectral data. For instance, in the case of compound **3**, the IR spectrum revealed absorption bands at 3267, 2977, 2915, and 1722 cm^{-1} corresponding to the NH, CH-aliphatic, and C = O (thiazinone) groups, respectively, and showed an absence of absorption bands at 3239, 3219, and 1719 cm^{-1} corresponding to the NH_2 and C = O (ester) groups. Additionally, in the ^1H NMR spectrum, a broad signal at 4.00 ppm and a singlet signal at 3.13 ppm were observed, which were attributed to the NH and CH_2 protons, respectively, and the absence of signals at 1.50, 4.20, and 6.40 ppm, which were attributed to the CH_3, CH_2 and NH_2 protons. Additionally, in the ^{13}C NMR spectrum, signals at 46.09 and 176.54 ppm were observed, which were attributed to the CH_2 and C = O (thiazinone) carbons, and the absence of signals at 12.34, 63.65, and 156.06 ppm, which were attributed to the CH_3, CH_2, and C = O (ester) carbons. For instance, in the case of compound **4**, the IR spectrum revealed absorption bands at 2853 and 1315 cm^{-1} corresponding to the CH-aliphatic and S = O groups, respectively, and showed an absence of an absorption band at 3267 cm^{-1} corresponding to the NH group. Additionally, in the ^1H NMR spectrum, a singlet signal at 2.60 ppm was observed, which was attributed to the CH_3 protons, and the absence of signal at 4.00 ppm, which was attributed to the NH proton. Additionally, in the ^{13}C NMR spectrum, a signal at 45.89 ppm was observed, which was attributed to the CH_3 carbon. Compound **2** underwent an efficient transformation to yield ethyl 5-oxo-6-phenyl-9-(1*H*-tetrazol-1-yl)-6,6a-dihydro-5*H*-thieno[2′,3′:4,5]thiazolo[3,2-*a*]quinazoline-8-carboxylate (**5**). This transformation was accomplished by reacting compound **2** with triethyl orthoformate and sodium azide in glacial acetic acid. The resulting compound **5** was then treated with hydrazine hydrate, leading to the successful synthesis of the cyclized diamino pyrimidinone **6**, which was obtained in good yield. The confirmation of the chemical structures of compounds **5** and **6** was achieved through the analysis of both analytical and spectral data. For instance, in the case of compound **5**, the IR spectrum revealed absorption bands at 1536 and 1408 cm^{-1}, corresponding to the C = N and N = N groups, and the absence of absorption bands at 3239 and 3219

https://doi.org/10.1021/acsomega.4c11076
ACS Omega 2025, 10, 9703−9717

cm^{-1}, corresponding to the NH_2 group. Additionally, in the ^1H NMR spectrum, a singlet signal at 9.48 ppm was observed, which was attributed to the CH tetrazole proton, and the absence of a broad signal at 6.40 ppm, which was attributed to the NH_2 protons. Additionally, in the ^{13}C NMR spectrum, a signal at 135.05 ppm was observed, which was attributed to the C = N tetrazole carbon. For instance, in the case of compound **6**, the IR spectrum revealed absorption bands at 3440, 3388, 1687, and 1631 cm^{-1}, corresponding to the $2NH_2$, C = O (pyrimidine), and C = N groups, respectively. Additionally, in the ^1H NMR spectrum, a broad signal at 6.18 ppm was observed, which was attributed to the $2NH_2$ group protons, and the absence of signals at 1.85, 4.25, and 9.48 ppm, which were attributed to the CH_3, CH_2 and CH tetrazole protons. Additionally, in the ^{13}C NMR spectrum, signals at 12.12, 63.07, 135.05, and 156.05 ppm disappeared, which were attributed to the $COOCH_2CH_3$ and C = N tetrazole ester carbons, and signals at 150.67 and 168.53 ppm were observed, which were attributed to the C = N and C = O (pyrimidine) carbons.

The fusion of compound **6** with two types of aromatic aldehydes, specifically 4-dimethylaminobenzaldehyde and furfuraldehyde, in an oil bath at 180 °C resulted in the formation of the desired triazolo-N,N-dimethylaniline and furan dihydrotriazole derivatives (**7**) and (**8**) (Scheme 3).The

Scheme 3. Synthesis of [1,2,4]Triazolo[1‴,5‴:1″,2″]pyrimido[5″,4″:4′,5′]thieno-[2′,3′:4,5]thiazolo[3,2-*a*]quinazoline-5,8-diones 7−10

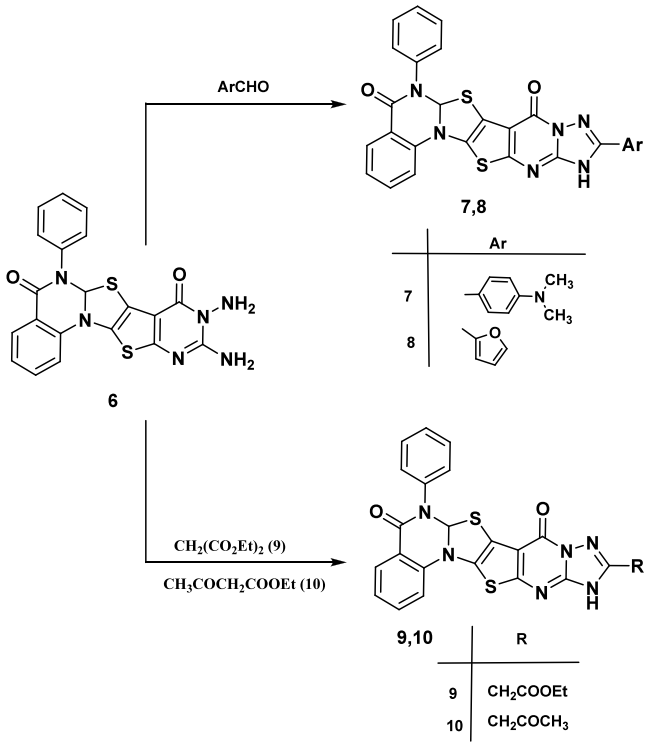

confirmation of the chemical structures of compounds **7** and **8** was achieved through the analysis of both analytical and spectral data. For instance, in the case of compound **7**, the IR spectrum revealed absorption bands at 3138, 2990, and 2947 cm^{-1}, corresponding to the NH and CH-aliphatic groups, respectively, and the absence of absorption bands at 3440 and 3388 cm^{-1}, corresponding to the NH_2 group. Additionally, in the ^1H NMR spectrum, singlet signals at 2.52 and 3.04 ppm were observed, which were attributed to the CH_3 and NH protons, and the absence of a signal at 6.18 ppm, which was attributed to the NH_2 protons. Additionally, the MS spectrum showed a molecular ion peak at m/z 563 [M+], corresponding to $C_{29}H_{21}N_7O_2S_2$, which aligns with the molar mass of the proposed structure. The primary fragmentation occurred at m/z 429, resulting from the loss of a $C_8H_{10}N_2$ group, corresponding to a (134 Da) mass loss, m/z = 365, indicating the loss of a C_2N_2O group (68 Da) and gaining 4 hydrogens, m/z = 293, indicating the loss of a C_2H_2NS group (72 Da), m/z = 227, indicating the loss of a -C_3S group (68 Da) and gaining 2 hydrogens, m/z = 170, indicating the loss of a C_2H_3NO group (57 Da), m/z = 110 indicating the loss of a C_5 group (60 Da), m/z = 94 indicating the loss of a CH_4 group (16 Da) and m/z = 81, indicating the loss of a CH group (13 Da) with 100% abundance as a base peak. In the case of compound **8**, the IR spectrum revealed an absorption band at 3186 cm^{-1}, corresponding to the NH group, and the absence of absorption bands at 3440 and 3388 cm^{-1}, corresponding to the NH_2 group. Additionally, in the ^1H NMR spectrum, singlet signals at 2.08 and 8.37 ppm were observed, which were attributed to NH and CH furfural protons. Additionally, the MS spectrum revealed a molecular ion peak at m/z 510 [M^+], corresponding to $C_{25}H_{14}N_6O_3S_2$ and in agreement with the molar mass of the suggested structure. The primary fragmentation occurred at m/z = 487 due to the loss of a CO group, corresponding to a (28 Da) mass loss and gaining 5 hydrogens, m/z = 440, indicating the loss of a CH_4O_2 group (48 Da), m/z = 339, indicating the loss of a C_5N_3 group (102 Da) and gaining 1 hydrogen, m/z = 227 indicating the loss of a $C_4H_4N_2S$ group (112 Da) with 100% abundance as a base peak, m/z = 120, indicating the loss of a C_6H_3S group (107 Da) and m/z = 57 indicating the loss of a C_5H_3 group (63 Da). Upon heating compound **6** with diethylmalonate, the ethyl acetate ester (**9**) was formed. The IR spectrum of compound **9** displayed prominent absorption bands at 3242, 2988, 2949, 2919, 2860, and 1788 cm^{-1} due to NH, CH aliphatic, and ester C = O groups, and the absence of absorption bands at 3440 and 3388 cm^{-1}, corresponding to the NH_2 group. In the ^1H NMR spectrum, broad and triplet signals appeared at 2.07 and 2.58 ppm, which were ascribed to the NH and methyl protons, singlet and quartet signals appeared at 3.15 and 4.20 ppm, which were ascribed to the two CH_2 protons, and there was an absence of signal at 6.18 ppm, which was attributed to the NH_2 protons. In the ^{13}C NMR spectrum, a signal at 15.39 ppm appeared, which was ascribed to the methyl carbon; 44.63 and 62.29 ppm appeared, which were ascribed to the $2CH_2$ carbons; and 169.08 ppm appeared, which was ascribed to the C = O (ester) carbon. The MS spectrum revealed a molecular ion peak at 530 m/z [M^+], corresponding to $C_{25}H_{18}N_6O_4S_2$ and in agreement with the molar mass of the suggested structure. The primary fragmentation occurred at m/z = 475 due to the loss of a C_2O_2 group, corresponding to a (55 Da) mass loss and gaining 1 hydrogen, m/z = 340, indicating the loss of a $C_7H_5NO_2$ group (135 Da), m/z = 274, indicating the loss of a $C_3H_2N_2$ group (66 Da) with 100% abundance as a base peak, m/z = 230, indicating the loss of a CS group (44 Da), m/z = 146, indicating the loss of a C_3H_2NS group (84 Da), and m/z = 69, indicating the loss of a C_4HN_2 group (77 Da). The synthesis of the triazolo propanone derivative (10) was successfully achieved with a satisfactory yield by reacting compound 6 with ethyl acetoacetate at 180

https://doi.org/10.1021/acsomega.4c11076
ACS Omega 2025, 10, 9703−9717

Scheme 4. Synthesis of [1,2,4]Triazolo[1‴,5‴:1″,2″]pyrimido[5″,4″:4′,5′]thieno[2′,3′:4,5]thiazolo[3,2-*a*]quinazoline-5,8-dione 11

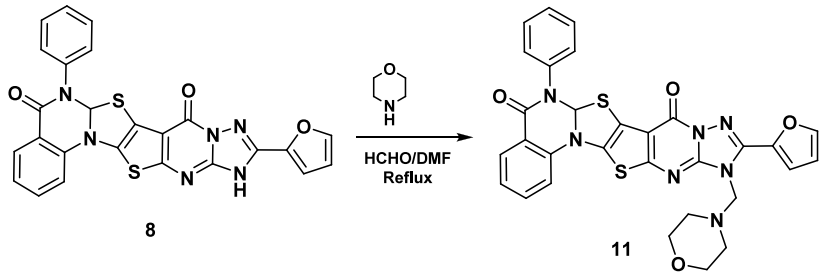

Scheme 5. Synthesis of [1,2,4]Triazolo[1‴,5‴:1″,2″]pyrimido[5″,4″:4′,5′]thieno[2′,3′:4,5]thiazolo[3,2-*a*]quinazoline-5,8-dione 12

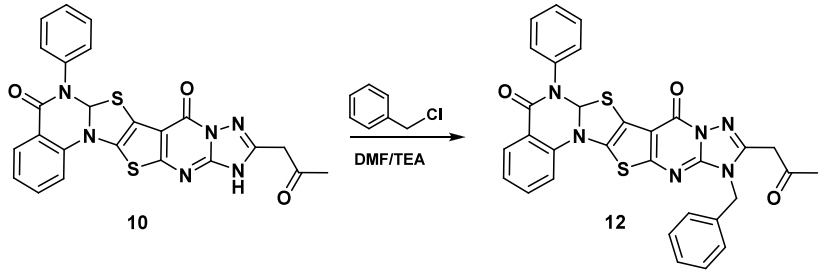

°C. The IR spectrum of compound **10** displayed prominent absorption bands at 3111, 2956, 2921, and 1740 cm^{-1} due to NH, CH aliphatic, and acetyl C = O groups, and the absence of absorption bands at 3440 and 3388 cm^{-1}, corresponding to the NH_2 group. In the ^1H NMR spectrum, broad, singlet signals appeared at 2.07, 2.58, and 4.31 ppm, which were ascribed to the NH, CH_3, and CH_2 protons, and there was an absence of signal at 6.18 ppm, which was attributed to the NH_2 protons. In the ^{13}C NMR spectrum, 27.20, 40.00, and 202.00 ppm appeared, which were ascribed to the CH_3, CH_2, and C = O carbons.

In Scheme 4, the desired 4-ethylmorpholine derivative **11** was prepared in 80% yield by reacting **8** with formaldehyde and morpholine in dry DMF to yield 11-(furan-2-yl)-12-(morpholinomethyl)-6-phenyl-6,6a-dihydro[1,2,4]triazolo-[1‴,5‴:1″,2″]pyrimido[5″,4″:4′,5′]thieno[2′,3′:4,5]thiazolo-[3,2-*a*]quinazoline-5,8(12*H*)-dione (**11**). The confirmation of the chemical structure of compound **11** was accomplished through the analysis of both analytical and spectral data. For example, in the case of compound **11**, the IR spectrum revealed absorption bands at 2992 and 2892 cm^{-1} corresponding to the CH-aliphatic group and the absence of an absorption band at 3186 cm^{-1}, corresponding to the NH group. Additionally, in the ^1H NMR spectrum, triplet signals at 2.31, 3.50, and 3.58 ppm were observed, which were attributed to the $4CH_2$ morpholine protons, respectively, and a singlet signal at 4.24 ppm was observed, which was attributed to the CH_2 protons, and the absence of a signal at 2.08 ppm, which was attributed to the NH proton. Additionally, in the ^{13}C NMR spectrum, signals at 55.57, 55.95, 59.50, and 67.20 ppm were observed, which were attributed to the $5CH_2$ carbons.

In Scheme 5, the desired benzyl derivative **12** was prepared in high yields by the reaction of **10** with benzyl chloride in the presence of triethylamine in dry DMF to yield 12-Benzyl-11-(2-oxopropyl)-6-phenyl-6,6a-dihydro-5*H*-[1,2,4]triazolo-[1‴,5‴:1″,2″]pyrimido[5″,4″:4′,5′]thieno[2′,3′:4,5]thiazolo-[3,2-*a*]quinazoline-5,8(12*H*)-dione (**12**). The confirmation of the chemical structure of compound **12** was achieved through the analysis of both analytical and spectral data. For instance, in the case of compound **12**, the IR spectrum showed absorption bands at 2989, 2945, 2921, and 1744 cm^{-1} corresponding to the CH-aliphatic and C = O groups, respectively, and the absence of an absorption band at 3111 cm^{-1}, corresponding to the NH group. Additionally, in the ^{13}C NMR spectrum, a signal at 34.56 ppm was observed, which was attributed to the CH_2−Ph ring carbon. Additionally, the MS spectrum revealed a molecular ion peak at 590 *m*/*z* [M^+], corresponding to $C_{31}H_{22}N_6O_3S_2$ and in agreement with the molar mass of the suggested structure. The primary fragmentation occurred at *m*/*z* = 454 due to the loss of a $C_5N_2O_3$ group, corresponding to a (136 Da) mass loss, *m*/*z* = 227, indicating the loss of a $C_{16}H_7N_2$ group (227 Da), *m*/*z* = 183, indicating the loss of a CS group (44 Da), *m*/*z* = 156, indicating the loss of a C_2H_3 group (27 Da), *m*/*z* = 113, indicating the loss of a C_3H_7 group (43 Da), and *m*/*z* = 62, indicating the loss of a C_2H_2 group (51 Da) with 100% abundance as a base peak.

2.2. Biological Activity. *2.2.1. Antimicrobial Efficiency.* The newly synthesized thiazolo-quinazoline derivatives **1**−**12** were evaluated in vitro for their antimicrobial activity. The evaluation targeted several pathogens versus *Staphylococcus aureus* (ATCC 25923) and methicillin-resistant *Staphylococcus aureus* (*MRSA*, USA300) as Gram-positive bacterial examples, *Escherichia coli* (ATCC 25922) as a Gram-negative bacterial example, and *Aspergillus fumigatus* (RCMB 002008) as a fungal example. The antimicrobial activity was initially screened using the agar diffusion method.[55−58] Ketoconazole and gentamicin were employed as reference drugs for antifungal and antibacterial activity, respectively. The results were recorded as the average diameters of inhibition zones (IZ) in millimeters, indicating the extent of bacterial or fungal growth suppression around the discs. These inhibition zone diameters were recorded based on a preliminary test, which is shown in Table S1 and Figure S1.

https://doi.org/10.1021/acsomega.4c11076
ACS Omega 2025, 10, 9703−9717

The obtained results showed that all screened derivatives exhibited no fungal activity against *Aspergillus fumigatus*. They produced moderate to mild inhibition zones against *S. aureus* (ATCC 25923) and *E. coli* (ATCC 25922) compared with gentamycin as a positive control. Regarding *MRSA* USA300, all compounds revealed no activity except **4** and **5** (IZ= 14 ± 0.22 and 17 ± 0.10 mm, respectively).

By calculation of MIC values for the promising derivatives as depicted in Table 1, it was noted that derivatives **4** and **5** revealed promising activity against *S. aureus* (ATCC 25923) and *MRSA* (USA300), however, compounds **2**, **3**, and **12** displayed potential potency against *E. coli* (ATCC 25922).

Table 1. MIC Values of the Promising Thiazolo-quinazoline Analogs in μM[a]

	MIC (Mean ± SEM) (μM)		
	Gram + ve Bacteria		Gram -ve Bacteria
Compd. No.	*S. aureus*(ATCC 25923)	MRSA (USA 300)	*E. coli*(ATTC 25922)
Gentamycin	2.5 ± 0.10	2.00 ± 0.15	3.2 ± 0.15
2	–	–	5.90 ± 0.22
3	–	–	2.95 ± 0.13
4	4.97 ± 0.24	5.90 ± 0.13	–
5	2.44 ± 0.17	3.32 ± 0.18	–
12	–	–	4.23 ± 0.25

[a]–: No activity.

Structure–Activity Relationship (SAR). The existence of the thieno-thiazolo-quinazoline scaffold in **2**, fused with the thiazine moiety in **3** or with the 12-benzyl-11-(2-oxopropyl)-triazolo-pyrimidine moiety in **12,** potentiates potency against *E. coli* (MIC = 5.90, 2.95, and 4.23 μM, respectively) compared with gentamycin (MIC = 3.2 μM). Substitution of the thiazine moiety in **3** with the methyl sulfonyl fragment in **4** altered activity toward *S. aureus* (ATCC 25923) and *MRSA* (USA300) (MIC = 4.97 and 5.90 μM, respectively) in comparison with the reference (MIC = 2.50 and 2.00 μM, respectively). Furthermore, superior potency was achieved against the latter strains upon substitution of thieno-thiazolo-quinazoline in **2** with a tetrazole moiety at p-9 in **5** (MIC = 2.44 and 3.32 μM, respectively). Enlargement of thieno-thiazolo-quinazoline through fusion or substitution with other moieties drastically decreased potency against all screened strains.

2.2.2. Effect of Compounds 4 and 5 on MRSA USA300 Biofilm Activity. The antibiofilm activity of the promising compounds **4** and **5** was investigated following the reported methodology.[59−61] Both compounds significantly inhibited and detached MRSA USA300 biofilm formation at all tested concentrations (two-way ANOVA, Tukey's posthoc test, $P < 0.05$) (Figure 3A&B). Compound **5** was more effective than compound **4** in MRSA biofilm inhibition activity with mean IC_{50} values of 0.263 and 0.786 μM, respectively. Regarding MRSA biofilm detachment activity, the same pattern was observed with mean DC_{50} values of 0.488 and 0.392 μM for compounds **4** and **5**, respectively.

2.2.3. In-Vivo MRSA Skin Infection Model. The MRSA skin infection model[62,63] was used to assess the *in vivo* antibacterial activity of thiazolo-quinazoline **4** and **5**. Both derivatives significantly reduced MRSA USA300 bacterial count compared to vehicle and negative control groups (one-way ANOVA, Tukey's posthoc test, $P < 0.0001$). Compound **5** had slightly higher *in vivo* activity than compound **4**, but there was no significant difference. The bacterial count recovered was 3.009 and 3.066 logs from the compound **4** group and 3.585 and 3.642 logs from the compound **5** group, lower than those of the untreated (negative control) and vehicle control (DMSO) groups, respectively (Figure 4A&B).

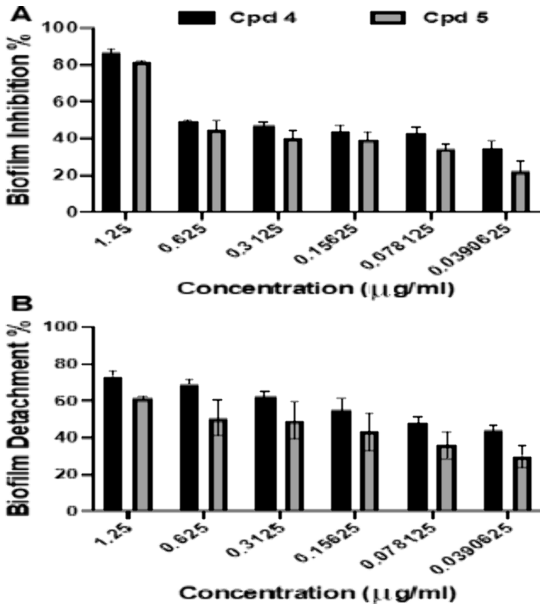

Figure 3. Antibiofilm activity: The effect of various subminimum bactericidal concentrations (MBC) (1.25−0.0390625 μg/mL) of compounds **4** and **5** on MRSA USA300 biofilm was evaluated. The results are presented as the mean biofilm inhibition percentage (**A**) ± standard error and the mean biofilm detachment percentage (**B**) ± standard error.

The promising thiazolo-quinazolines **4** and **5** were further evaluated for their inhibitory activities against *S. aureus* DNA gyrase to predict their mechanism of action, comparing them with the standard ciprofloxacin. The obtained results, expressed as IC50 values in μM, were collected for analysis in Table 2 and Figure S2.

Both derivatives **4** and **5** demonstrated excellent and superior inhibitory potency against *S. aureus* DNA gyrase compared to the reference ciprofloxacin, with IC50 values of 11.72 ± 0.47, 7.13 ± 0.28, and 19.3 ± 0.73 μM, respectively

2.3. Computational Studies. *2.3.1. Docking Application.* Based upon the amazing *in vitro* inhibitory potencies against *S. aureus* DNA gyrase, a docking simulation of potential thiazolo-quinazolines **4** and **5** was conducted using Auto Dock Vina 4.2 software to determine the anticipated binding affinities with *Staphylococcus aureus* DNA gyrase (PDB ID: 2XCT).[64] The X-ray crystallographic structure of *S. aureus* DNA gyrase and its natural ligand, ciprofloxacin, was obtained by accessing a protein data bank. We first redocked the original ligand ciprofloxacin inside its receptor to validate the docking procedure. This resulted in a small RMSD value of 0.85 Å between the docked pose and the cocrystallized ligand, as well as an energy score of −11.58 kcal/mol.

With high energy scores of −10.93 and −11.25 kcal/mol, respectively, thiazolo-quinazolines **4** and **5** were well placed within *S. aureus* DNA gyrase, as seen in Figures 5 and 6. Sulfur of the thiazine moiety and sulfonyl oxygens in **4** afforded four H-bonding with **His1081**, **Val511**, **Asp512,** and **Arg1033**

https://doi.org/10.1021/acsomega.4c11076
ACS Omega 2025, 10, 9703−9717

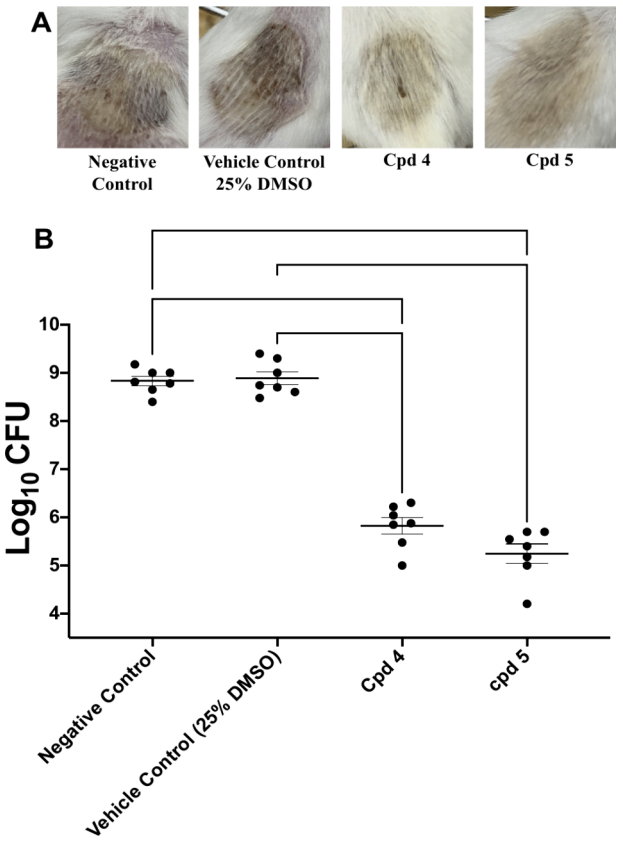

Figure 4. Efficacy of compounds **4** and **5** in an in vivo murine model of MRSA skin infection: Twenty-eight BALB/C mice were divided into four groups (n = 7). **A**: Photographic image showing the efficacy of different treatment groups on MRSA skin infection on the posterior backs of mice at the end of the experiment. **B**: Efficacy of different treatment groups on bacterial load in the murine model of MRSA skin infection. Each data point represents a mouse. Results are expressed as mean ± standard error. **** indicates a significant difference at $p <$ 0.0001 (one-way ANOVA, Tukey's posthoc test).*2.2.4. In-vitro assay against S. aureus* DNA gyrase.

Table 2. Evaluation of the Inhibitory Activities of the Selected Thiazolo-quinazolines 4 and 5, in Comparison with Ciprofloxacin, Against *S. aureus* DNA Gyrase[a]

	$IC_{50}(\mu M)$ (mean ± SEM)
Compd. No.	***S. aureus* DNA gyrase supercoiling**
4	11.72 ± 0.47
5	7.13 ± 0.28
Ciprofloxacin	19.3 ± 0.73

[a]IC50: The compound concentration required to inhibit 50% of the enzyme activity, represented by the standard error of the mean (SEM). Each value corresponds to the average of three readings.

(distances: 3.06, 2.53, 2.67, and 1.95 Å, respectively). Also, molecule **4** shared hydrophobic contacts with **Asp510**, **Tyr580**, **Lys581**, **Pro1080**, and **His 1081** (Figure 5A&B).

On the other hand, the nitrogen of tetrazole and the carbonyl oxygen of ethyl carboxylate in derivative **5** displayed H-bond acceptors with **Arg1033** and **His1081** (distances: 2.46 and 1.99 Å, respectively). Additional hydrophobic interactions were observed with **Asp508**, **Asp510**, **Val511**, and **Asp512** (Figure 6A&B).

According to previous findings, the thieno-thiazolo-quinazoline core that was attached to the thiazine-methylsulfonyl fragment in **4** or tetrazole-ethyl carboxylate in **5** enabled fitting within *S. aureus* DNA gyrase active site by H-bonding with essential amino acids **Arg1033** and **His1081**.

2.3.2. In Silico Prediction of ADMET. Using the free Web sites SwissADME and admetSAR 1.0, the appealing thieno-thiazolo-quinazolines **4** and **5** were further investigated for their expected pharmacokinetic, physicochemical, and toxicological characteristics.[32,65−69]

The optimal medication choice can be determined by analyzing the ADMET properties (absorption, distribution, metabolism, excretion, and toxicity) of the targeted drugs.-Veber and Lipinski's principles could identify the best drug to take orally. The thieno-thiazolo-quinazolines **4** and **5** only violated the Veber rule once (TPSA > 140), while derivative **4** additionally displayed a violation of Lipinski's principle (MW > 500) (Table 3).

The evaluated thieno-thiazolo-quinazolines **4** and **5** fall within the ideal range (pink zone) for key features (solubility, lipophilicity, flexibility, and size) on the bioavailability radar map (Figure 7), except for polarity and saturation.

An admet SAR 1.0 analysis of ADMET associated with potential thieno-thiazolo-quinazolines **4** and **5** is shown in Table S2. These substances had no chance of passing through the blood-brain barrier and had a limited likelihood of gastrointestinal absorption. As a result, they could be used to treat peripheral illnesses without triggering central problems. Transporter for drug efflux P-glycoprotein, or P-gp, serves in the responsibility of eliminating medications from cells and may influence drug tolerance. Since they are not P-gp substrates, the tested thieno-thiazolo-quinazolines **4** and **5** show minimal discharge from cells with the greatest activity. In the mitochondria, both are also dispersed and concentrated.

Research has shown that blocking more CYP enzymes raises the risk that a drug would interact with other active molecules in drug−drug interactions (DDI).[70,71] It was therefore expected that the majority of CYPs would not be significantly affected by these medications.

With no Ames toxicity, target **4** failed to block the potassium channel associated with the human ether-a-go-go gene (hERG) as expected. This suggests that there may not be much of a risk for genotoxicity or cardiotoxicity, which are common concerns during clinical trials for pharmaceutical candidates, but **5** did not.

Furthermore, based on estimates of acute oral toxicity, thieno-thiazolo-quinazolines **4** and **5** yielded readings of 634.6 and 656.8 $mg.kg^{-1}$, respectively. These results were classified as harmless compounds since they fell into the third group (500 $mg.kg^{-1} < LD_{50} \leq 5000\ mg.kg^{-1}$).

According to their carcinogenicity descriptor (CARC) values, which are 606.6 and 513.3 mg/kg^{-1} body weight per day, respectively, these compounds may also be classified as noncarcinogenic and nonrequired. When derivative **5**'s ability to decompose in the environment was evaluated, it was anticipated that it would be considered nonbiodegradable, but derivative **4** would not.

2.3.3. Quantum Chemical Calculation. Quantum chemical properties of the 12 synthetic compounds are described in the data in Table S3, with particular attention paid to the energy gap (ΔE), HOMO, and LUMO energies. When evaluating their stability, reactivity, and possible biological activity.

The HOMO−LUMO energy gap (ΔE) is a crucial quantum parameter. The ease of electron transmission is indicated by ΔE, which is the difference between the HOMO and LUMO

https://doi.org/10.1021/acsomega.4c11076
ACS Omega 2025, 10, 9703−9717

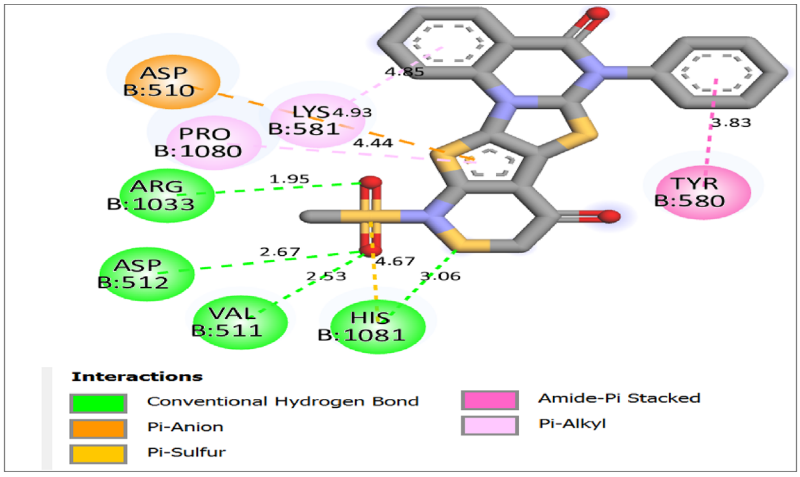

A

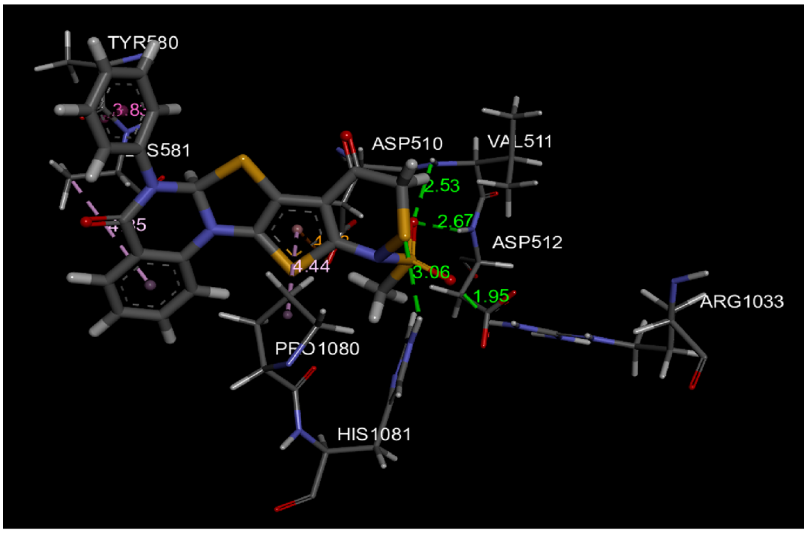

B

Figure 5. A and B patterns display the two- and three-dimensional binding poses of the promising thiazolo-quinazoline **4** within the active pocket of *Staphylococcus aureus* DNA gyrase (PDB ID: 2XCT).

energy levels. Higher reactivity is suggested by smaller ΔE values because electronic excitation is simpler. The distribution of electron density across the molecule is seen in ESP maps. Low-density regions (positive ESP) are conducive to nucleophilic attack, whereas regions with high electron density (negative ESP) indicate places vulnerable to electrophilic attack. To increase their antibacterial potency, compounds with different ESP distributions may bind to microbial cell components like proteins or DNA in a specific manner. From the table that we discovered, Compound **5** has the minimum ΔE of 0.01893 eV, which indicates great chemical reactivity, and Compound **1** exhibits the greatest ΔE of 0.06387 eV, indicating comparatively lesser reactivity.

Compounds with smaller ΔE values are more likely to interact with biological targets, such as enzymes or cell membranes, potentially disrupting microbial processes. Compounds **5** and **7** are particularly notable due to their low ΔE, which might translate into stronger antimicrobial activity.

Smaller ΔE values increase the likelihood that a compound may interact with biological targets, like cell membranes or enzymes, and may interfere with microbiological functions. Because of their low ΔE, which may indicate higher antibacterial activity, compounds **5** and **7** stand out.

The following insights for antimicrobial prediction are obtained from the combined examination of HOMO, LUMO, ΔE, and ESP: Low ΔE Compounds: High reactivity is probably exhibited by compounds **5**, **7**, and **4**, allowing for effective interaction with microbial targets like membrane proteins or enzymes. These interactions may cause antimicrobial effects by interfering with metabolic processes or disrupting the formation of microbial cell walls. Compounds with moderate LUMO values (e.g., Compounds **6**, **8**, **10**) could act as inhibitors by binding electron-rich microbial enzymes.

High HOMO values, such as in Compound **5**, may allow interaction with oxidative stress sites, leading to microbial cell damage. Potential for Selective Toxicity: If available, ESP maps can forecast which microbial targets will bind more selectively than mammalian cells, potentially lowering cytotoxicity.

Because of their low ΔE values and advantageous HOMO−LUMO properties, compounds **5** and **7** are the most promising antimicrobial candidates. To confirm these predictions and

https://doi.org/10.1021/acsomega.4c11076
ACS Omega 2025, 10, 9703−9717

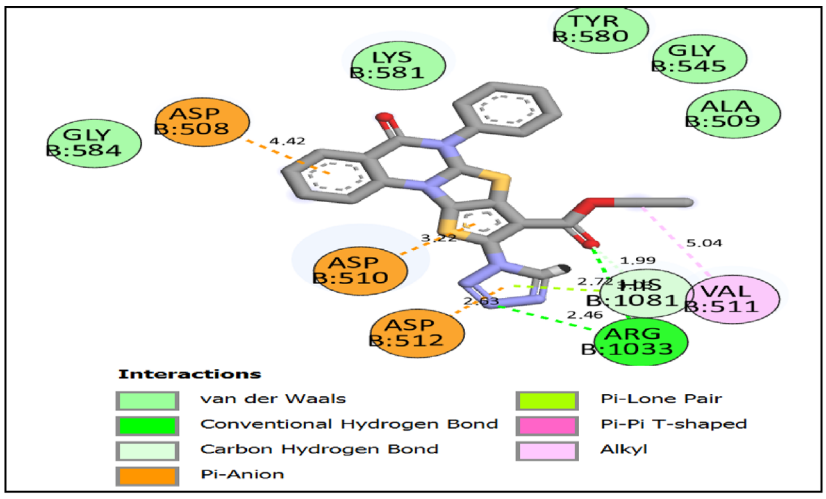

A

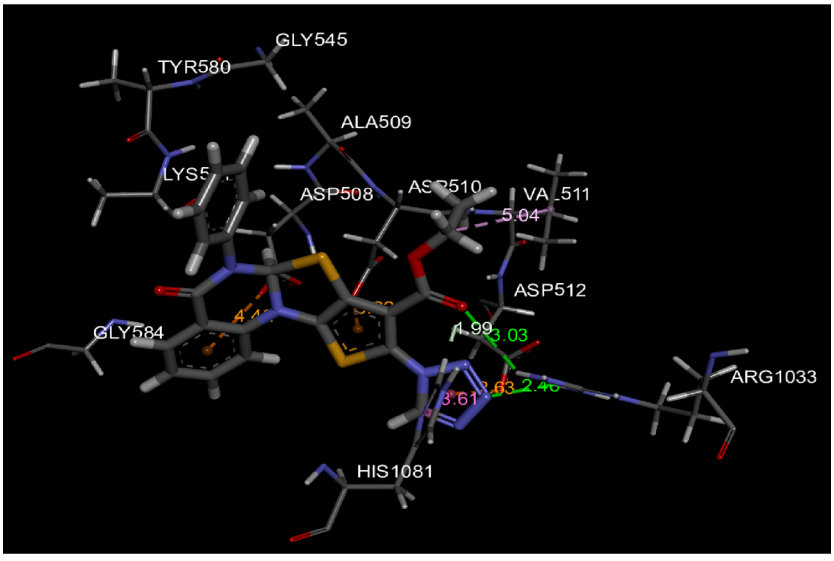

B

Figure 6. A and B views illustrate the two- and three-dimensional binding poses of thiazolo-quinazoline **5** in the active pocket of *Staphylococcus aureus* DNA gyrase (PDB ID: 2XCT).

Table 3. Calculated Physicochemical Characteristics of Attractive Thieno-thiazolo-quinazolines 4 and 5

Compd.	MW[a]	TPSA (Å^2)[b]	nRB[c]	nHBA[d]	nHBD[e]	MLogP[f]	Violations[g]
Rule	≤500	≤140	≤10	≤10	≤5	≤4.15	-
4	501.62	165.22	2	4	0	2.00	1 (Lipinski) MW > 500; 1 (Veber) TPSA > 140
5	476.53	146.99	5	6	0	3.72	0 (Lipinski) 1 (Veber) TPSA > 140

[a]Molecular weight. [b]Topological polar surface area. [c]Number of rotatable bonds. [d]Number of hydrogen bond acceptors. [e]Number of hydrogen bond donors. [f]Calculated lipophilicity (MLog Po/w). [g]Violations from Lipinski and Veber rules.

ascertain the compounds' specificity and potency, additional research is required, including molecular docking and in vitro antimicrobial assays (Figure 8).

3. CONCLUSIONS

Novel quinazoline-4-one derivatives were designed, synthesized, and evaluated for their in vitro antimicrobial activity against a variety of pathogens, including Gram-negative bacteria (*Escherichia coli* ATCC 25922), Gram-positive bacteria (*Staphylococcus aureus* ATCC 25923 and methicillin-resistant *Staphylococcus aureus* [MRSA, USA300]), and fungi (*Aspergillus fumigatus* RCMB 002008). Among the derivatives, the thieno-thiazolo-quinazoline compounds **4** and **5** demonstrated significant activity, effectively inhibiting and disrupting MRSA USA300 biofilm formation across various concentrations.

To assess their effectiveness further, an *in vivo* MRSA skin infection model was utilized, highlighting the potential of these derivatives against MRSA. To provide deeper insights into their mode of action, ADMET profiling and molecular docking

https://doi.org/10.1021/acsomega.4c11076
ACS Omega 2025, 10, 9703−9717

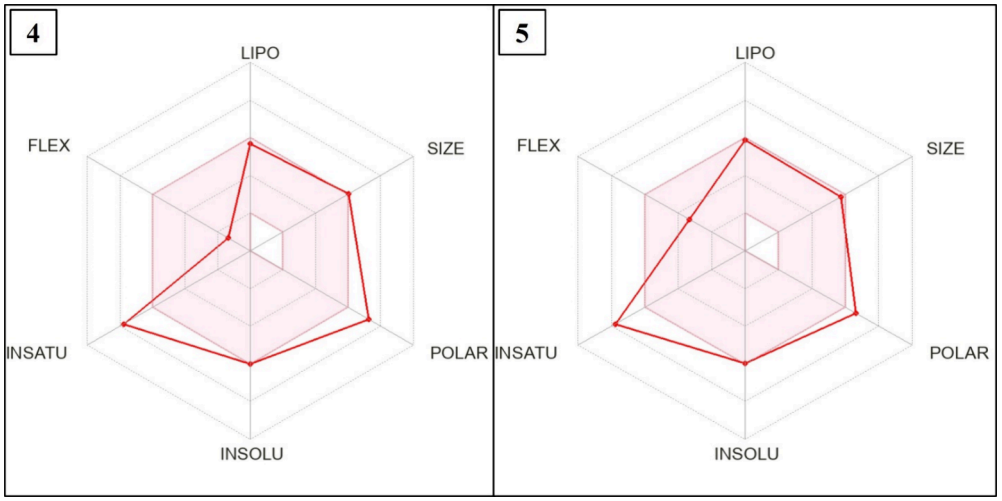

Figure 7. Bioavailability radar map of the significant thieno-thiazolo-quinazolines **4** and **5**. The pink region represents the optimal values for each component of oral bioavailability, while the red lines indicate the expected values for the studied targets.

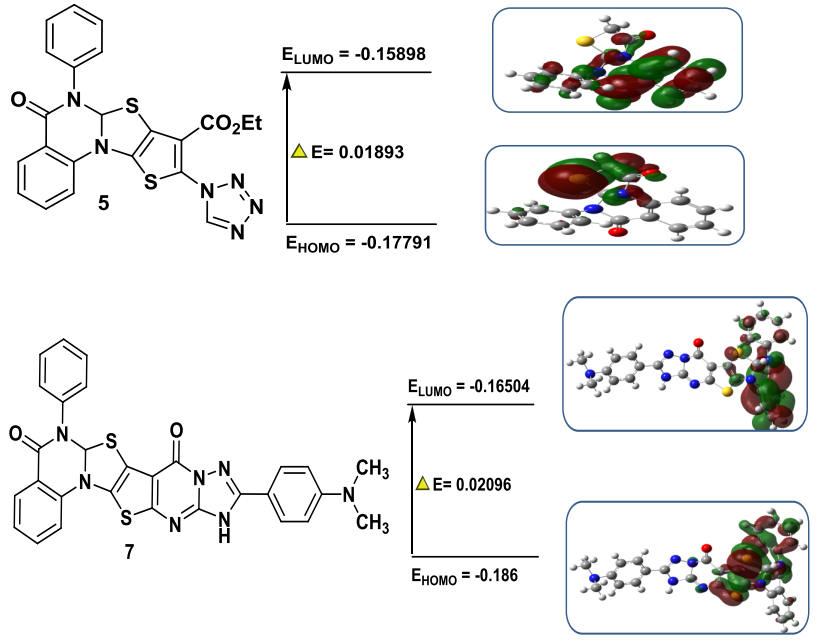

Figure 8. DFT-optimized structures and HOMO/LUMO (Highest Occupied Molecular Orbital/Lowest Unoccupied Molecular Orbital) diagrams of compounds **5** and **7**.

simulations were performed to investigate the binding interactions between the promising compounds and *Staphylococcus aureus* DNA gyrase, the target enzyme.

4. EXPERIMENTAL SECTION

4.1. Chemistry. All details of apparatuses used in spectral analyses were mentioned in the supplementary file.

*4-Phenyl-3a,4-dihydro-5H-thiazolo[3,2-a]quinazoline-1,5(2H)-dione (**1**).* A solution of **A** (2.54 g, 10 mmol) in 1,4-dioxane (20 mL) was refluxed with chloroacetic acid (0.6 mL, 10 mmol) for 2 h. The reaction mixture was cooled and then poured in ice water. The solid product was filtered, washed, and recrystallized from ethanol to get **1** as a pale pink powder in a (72%) yield, mp 240−242 °C. IR (KBr) cm^{-1} ν_{max}: 3063 cm^{-1} (ν CH-Ar), 2936 cm^{-1} (ν CH aliphatic), 1730, 1648 cm^{-1} (ν C = O amide), 1618 cm^{-1} (C = C Ar). ^{1}H NMR (DMSO-d_6, 400 MHz,) δ= 4.16 (s, 2H, CH_2), 7.22 (s, 1H, CH-S), 7.23−7.48 (m, 9H, Ar−H) ppm. ^{13}C NMR (DMSO-d_6, 100 MHz) δ = 45.51 (1C, CH_2), 90.00 (1C, CH-S), 114.31−139.88 (11C, C−Ar), 150.20 (1C, C−N), 172.37, 162.33 (2C, 2C = O) ppm.

*Ethyl 9-Amino-5-oxo-6-phenyl-6,6a-dihydro-5H thieno-[2′,3′:4,5]thiazolo[3,2-a]quinazoline-8-carboxylate (**2**).* Sulfur (0.32 g, 10 mmol) was added slowly over 15 min to a mixture of compound **1** (2.96 g, 10 mmol) in DMF (20 mL), ethyl cyanoacetate (1.1 mL, 10 mmol), and diethylamine (1 mL, 10 mmol). The reaction mixture was stirred under reflux at 70 °C for 3 h. After cooling, the separated solid was filtered off, and the filtrate was evaporated under reduced pressure. The remaining residue was recrystallized from acetone to yield compound **2** as a gray powder in a 79% yield, mp 298−300 °C. IR (KBr) cm^{-1} ν_{max}: 3239, 3219 cm^{-1} (ν NH_2), 3064, 3028 cm^{-1} (ν CH-Ar), 1719, 1663 cm^{-1} (ν 2C = O), 1622 cm^{-1} (C = C Ar). 1H-NMR (DMSO-d_6, 400 MHz,) δ= 1.50 (t, J = 2.8

https://doi.org/10.1021/acsomega.4c11076
ACS Omega 2025, 10, 9703−9717

Hz, 3H, CH_3), 4.20 (q, J = 4.6 Hz, 2H, CH_2), 7.26 (s, 1H, CH-S), 6.40 (br, 1H, NH_2 exchangeable), 7.27−8.02 (m, 9H, Ar−H) ppm. ^{13}C NMR (DMSO-d_6, 100 MHz) δ = 12.34 (1C, CH_3), 63.65 (1C, CH_2), 91.95 (1C, CH-S), 111.08−144.44 (15C, Ar−C), 156.06, 163.92 (2C, 2C = O), 160.00 (1C, C-NH_2) ppm.

*Phenyl-6,6a-dihydro-5H,9H-[1,2]thiazino[4″,3″:4′,5′]thieno[2′,3′:4,5]thiazolo[3,2-a]quinazoline-5,8(11H)-dione (**3**).* A solution of **2** (4.23 g, 10 mmol) in DMF (20 mL) was refluxed with sulfur (2.56 g, 10 mmol) for 8 h. The reaction mixture was cooled and then poured in ice water. The solid product was filtered, washed, and recrystallized from methanol to get **3** as a gray powder in a (66%) yield, mp 255−257 °C. IR (KBr) cm^{-1} ν_{max}: 3267 cm^{-1} (ν NH), 3042 cm^{-1} (ν CH-Ar), 2977, 2915 cm^{-1} (ν CH aliphatic), 1722, 1668 cm^{-1} (ν 2C = O), 1631 cm^{-1} (C = C Ar). ^{1}H NMR (DMSO-d_6, 400 MHz,) δ= 4.00 (br, 1H, NH exchangeable), 3.13 (s, 2H, CH_2), 7.30 (s, 1H, CH-S), 7.32−7.98 (m, 9H, Ar−H) ppm. ^{13}C NMR (DMSO-d_6, 100 MHz) δ= 46.09 (1C, CH_2), 92.06 (1C, CH-S), 114.80−160.29 (16C, Ar−C), 162.69, 176.54 (2C, 2C = O) ppm.

*(Methylsulfonyl)-6-phenyl-6,6a-dihydro-5H,9H-[1,2]thiazino[4″,3″:4′,5′]thieno[2′,3′:4,5]thiazolo[3,2-a]quinazoline-5,8(11H)-dione (**4**).* A solution of **3** (4.23 g, 10 mmol) in DMF (20 mL) was stirred with methane sulfonyl chloride (0.8 mL, 10 mmol) in the presence of triethylamine (3 drops) for 24 h. The reaction mixture was cooled, then the solid product was filtered, washed, and recrystallized from ethanol to get **4** as a black crystals in (88%) yield, mp 220−222 °C. IR (KBr) cm^{-1} ν_{max}: 3099, 3057 cm^{-1} (ν CH-Ar), 2998, 2853 cm^{-1} (ν CH aliphatic), 1740, 1674 cm^{-1} (ν 2C = O), 1620 cm^{-1} (ν C = N), 1599 cm^{-1} (C = C Ar), 1315 cm^{-1} (ν S = O). ^{1}H NMR (DMSO-d_6, 400 MHz,) δ= 2.60 (s, 3H, CH_3), 3.10 (s, 2H, CH_2), 7.22 (s, 1H, CH-S), 7.24−7.97 (m, 9H, Ar−H) ppm. ^{13}C NMR (DMSO-d_6, 100 MHz) δ= 45.89 (2C, CH_2, CH_3), 90.00 (1C, CH-S), 114.78−160.29 (16C, Ar−C), 162.70, 176.52 (2C, 2C = O) ppm.

*Ethyl 5-Oxo-6-phenyl-9-(1H-tetrazol-1-yl)-6,6a-dihydro-5H-thieno[2′,3′:4,5]thiazolo[3,2-a]quinazoline-8-carboxylate (**5**).* Triethyl orthoformate (38 mL, 230 mmol) and sodium azide (3.9 g, 60 mmol) were added to a solution of **2** (21 g, 50 mmol) in glacial acetic acid (30 mL) and agitated under reflux for 2 h. After cooling the reaction mixture, 7 mL of HCl were added. After filtering out the solid product, the filtrate was evaporated at a lower pressure. To obtain **5** as a pale yellow powder, the leftover residue was recrystallized, cleaned, and then recrystallized from ethanol in a (76%) yield, mp 280−282 °C. IR (KBr) cm^{-1} ν_{max}: 3051 cm^{-1} (ν CH-Ar), 2914 cm^{-1} (ν CH aliphatic), 1726, 1651 cm^{-1} (ν 2C = O), 1536 cm^{-1} (ν C = N), 1469 cm^{-1} (ν C = C Ar), 1408 cm^{-1} (ν N = N). ^{1}H NMR (DMSO-d_6, 400 MHz,) δ= 1.85 (t, J = 6.8 Hz, 3H, CH_3), 4.25 (dd, J = 2.8 Hz, 2H, CH_2), 7.25 (s, 2H, CH-S), 7.37−8.15 (m, 9H, Ar−H), 9.48 (s, 1H, CH tetrazole) ppm. ^{13}C NMR (DMSO-d_6, 100 MHz) δ = 12.12 (1C, CH_3), 63.07 (1C, CH_2), 95.19 (1C, CH-S), 114.31−128.92 (14C, Ar−C), 135.05 (1C, C = N), 145.04 (1C, C−N), 151.00 (1C, C−S), 156.05, 163.02 (2C, 2C = O) ppm.

*9,10-Diamino-6-phenyl-6,6a-dihydro-5H-pyrimido[5″,4″:4′,5′]thieno[2′,3′:4,5]thiazolo[3,2-a]quinazoline-5,8(9H)-dione (**6**).* A solution of **5** (4.76 g, 10 mmol) in EtOH (20 mL) was refluxed with hydrazine hydrate (1.25 mL, 25 mmol) for 8 h. The reaction mixture was cooled and then poured in ice water. The solid product was filtered, washed, and recrystallized from chloroform to get **6** as a pale brown in (89%) yield, mp 216−218 °C. IR (KBr) cm^{-1} ν_{max}: 3440, 3388 cm^{-1} (ν 2NH_2), 3130 cm^{-1} (ν CH-Ar), 1687, 1631 cm^{-1} (ν 2C = O, C = N), 1525 cm^{-1} (C = C Ar). ^{1}H NMR (DMSO-d_6, 400 MHz,) δ= 6.18 (br, 2H, 2NH_2 exchangeable), 7.20 (s, 1H, CH), 7.33−8.86 (m, 9H, Ar−H) ppm. ^{13}C NMR (DMSO-d_6, 100 MHz) δ = 93.99 (1C, CH-S), 114.79−140.30 (16C, Ar−C), 150.67 (1C, C = N), 168.53, 160.29 (2C, C = O) ppm.

*11-[4-(Dimethylamino)phenyl]-6-phenyl-6,6a-dihydro-5H-[1,2,4]triazolo[1‴,5‴:1″,2″]pyrimido[5″,4″:4′,5′]thieno-[2′,3′:4,5]thiazolo[3,2-a]quinazoline-5,8(12H)-dione (**7**).* A mixture of **6** (4.34 g, 10 mmol) and dimethylaminobenzaldehyde (2.98 g, 20 mmol) was heated in an oil bath at 180 °C for 1 h. The reaction mixture was cooled, and 10 mL EtOH was added to the solidified mass. The solid product was filtered, washed, and recrystallized from ethanol to get **7** as a white powder in a (66%) yield, mp >300 °C. IR (KBr) cm^{-1} ν_{max}: 3138 cm^{-1} (ν NH), 3082, 3060 cm^{-1} (ν CH-Ar), 2990, 2947 cm^{-1} (ν CH aliphatic), 1690, 1670 cm^{-1} (ν 2C = O), 1618 cm^{-1} (ν C = N), 1602 cm^{-1} (C = C Ar). EI-MS: m/z ($C_{29}H_{21}N_7O_2S_2$) calcd = 562.9 [M+]. ^{1}H NMR (DMSO-d_6, 400 MHz,) δ= 2.52 (s, 6H, 2CH3), 3.04 (br, 1H, 1NH exchangeable), 7.05 (s, 1H, CH-S), 7.32−9.05 (m, 13H, Ar−H) ppm.

*11-(Furan-2-yl)-6-phenyl-6,6a-dihydro-5H-[1,2,4]triazolo-[1‴,5‴:1″,2″]pyrimido[5″,4″:4′,5′]thieno[2′,3′:4,5]thiazolo-[3,2-a]quinazoline-5,8(12H)-dione (**8**).* A mixture of **6** (4.34 g, 10 mmol) and furfuraldehyde (1.65 mL, 20 mmol) was heated in an oil bath at 180 °C for 1 h. The reaction mixture was cooled, and 10 mL EtOH was added to the solidified mass. The solid product was filtered, washed, and recrystallized from ethanol to get **8** as a gray powder in a (71%) yield, mp >300 °C. IR (KBr) cm^{-1} ν_{max}: 3186 cm^{-1} (ν NH), 3061 cm^{-1} (ν CH-Ar), 2977 cm^{-1} (ν CH aliphatic), 1701, 1664 cm^{-1} (ν 2C = O), 1619 cm^{-1} (ν C = N), 1522 cm^{-1} (C = C Ar). EI-MS: m/z ($C_{25}H_{14}N_6O_3S_2$) calcd = 510.2 [M$^+$]. ^{1}H NMR (DMSO-d_6, 400 MHz,) δ = 2.08 (br, 1H, 1NH exchangeable), 7.15 (s, 1H, CH-S), 7.18−8.13 (m, 11H, Ar−H), 8.37 (s, 1H, CH furfural) ppm.

*Ethyl 2-(5,8-Dioxo-6-phenyl-6,6a,8,12-tetrahydro-5H-[1,2,4]triazolo[1‴,5‴:1″,2″]pyrimido[5″,4″:4′,5′]thieno-[2′,3′:4,5]thiazolo[3,2-a]quinazolin-11-yl)acetate (**9**).* A suspension of **6** (4.34 g, 10 mmol) in diethylmalonate (1.63 g, 10 mmol) was refluxed for 6 h. The reaction mixture was cooled, then the solid product was filtered, washed, and recrystallized from ethanol to get **9** as a dark red powder in (74%) yield, mp 278−280 °C. IR (KBr) cm^{-1} ν_{max}: 3242 cm^{-1} (ν NH), 3049, 3024 cm^{-1} (ν CH-Ar), 2988, 2949, 2919, 2860 cm^{-1} (ν CH aliphatic), 1788, 1694, 1653 cm^{-1} (ν 3C = O), 1619 cm^{-1} (ν C = N), 1554 cm^{-1} (C = C Ar). EI-MS: m/z ($C_{25}H_{18}N_6O_4S_2$) calcd = 531.4 [M$^+$]. ^{1}H NMR (DMSO-d_6, 400 MHz,) δ= 2.01 (br, 1H, 1NH exchangeable), 1.50 (t, J = 2.6 Hz, 3H, CH3), 3.15 (s, 2H, CH2), 4.20 (q, J = 2.2 Hz, 2H, CH2), 7.06 (s, 1H, CH-S), 7.26−8.02 (m, 9H, Ar−H) ppm. ^{13}C NMR (DMSO-d_6, 100 MHz) δ = 15.39 (1C, CH_3), 44.63, 62.29 (2C, 2CH_2), 9.09 (1C, CH-S), 114.79−140.08 (166C, Ar−C), 158.67 (2C, 2C = N), 161.54, 163.33, 169.08 (3C, 3C = O).

*6−11-(2-Oxopropyl)-6-phenyl-6,6a-dihydro-5H-[1,2,4]-triazolo[1‴,5‴:1″,2″]pyrimido[5″,4″:4′,5′]thieno[2′,3′:4,5]-thiazolo[3,2-a]quinazoline-5,8(12H)-dione(**10**).* A suspension of **6** (4.34 g, 10 mmol) in ethyl acetoacetate (1.3 mL, 10 mmol) was refluxed for 6 h. The reaction mixture was cooled,

https://doi.org/10.1021/acsomega.4c11076
ACS Omega 2025, 10, 9703−9717

then the solid product was filtered, washed, and recrystallized from ethyl acetate to get **10** as an orange powder in (46%) yield, mp >300 °C. IR (KBr) cm-1 ν_{max}: 3111 cm^{-1} (ν NH), 3069, 3024 cm^{-1} (ν CH-Ar), 2956, 2921 cm^{-1} (ν CH aliphatic), 1740, 1671, 1613 cm^{-1} (ν 3C = O), 1587 cm^{-1} (ν C = N), 1487 cm^{-1} (C = C Ar). ^{1}H NMR (DMSO-d_6, 400 MHz,) δ= 2.07 (br, 1H, 1NH exchangeable), 2.58 (s, 3H, CH_3), 4.31, 4.39 (s, 2H, CH_2), 7.15 (s, 1H, CH-S), 7.18−8.13 (m, 9H, Ar−H) ppm. ^{13}C NMR (DMSO-d_6, 100 MHz) δ= 27.20 (1C, CH_3), 40.00 (1C, CH_2−CO), 95.57 (1C, CH-N), 111.01−140.00 (15C, Ar−C), 150.58, 151.00, 151.99 (3C, 3C = N), 162.02, 162.99, 202.00 (3C, 3C = O).

*11-(Furan-2-yl)-12-(morpholinomethyl)-6-phenyl-6,6a-dihydro-5H-[1,2,4]triazolo[1‴,5‴:1″,2″]pyrimido[5″,4″:4′,5′]-thieno[2′,3′:4,5]thiazolo[3,2-a]quinazoline-5,8(12H)-dione (**11**).* A solution of **8** (5.10 g, 10 mmol) in DMF (15 mL) was refluxed with formaldehyde (0.36 mL, 10 mmol) and morpholine (0.86 mL, 10 mmol) for 15 h. The reaction mixture was poured onto ice. The formed precipitate was filtered off, washed, and recrystallized from DMF to get **11** as an off-white powder in (48%) yield, mp >300 °C. IR (KBr) cm^{-1} ν_{max}: 3050 cm^{-1} (ν CH-Ar), 2992, 2892 cm^{-1} (ν CH aliphatic), 1696, 1658 cm^{-1} (ν 2C = O), 1608 cm^{-1} (ν C = N), 1586 cm^{-1} (C = C Ar). ^{1}H NMR (DMSO-d_6, 400 MHz,) δ = 2.31 (t, J = 6.4 Hz, 4H, $2CH_2$−N), 3.50, 3.58 (t, J = 3.00 Hz, 4H, $2CH_2$−O), 4.24 (s, 2H, CH_2), 7.07 (s, 1H, CH-S), 7.19−8.58 (m, 12H, Ar−H) ppm. ^{13}C NMR (DMSO-d_6, 100 MHz) δ = 55.57, 55.95 (2C, $2CH_2$−N), 59.50 (1C, CH_2), 67.20 (2C, $2CH_2$−O), 95.95 (1C, CH-S), 111.08−144.44 (21C, Ar−C), 156.06 (1C, C−S pyrimidine), 161.00, 161.29 (2C, 2C = O).

*12-Benzyl-11-(2-oxopropyl)-6-phenyl-6,6a-dihydro-5H-[1,2,4]triazolo[1‴,5‴:1″,2″]pyrimido[5″,4″:4′,5′]thieno-[2′,3′:4,5]thiazolo[3,2-a]quinazoline-5,8(12H)-dione (**12**).* A solution of **10** (5 g, 10 mmol) in DMF (20 mL) was stirred with benzyl chloride (1.15 mL, 10 mmol) in the presence of triethylamine (3 drops) overnight. The reaction mixture was poured into ice water. The solid product was filtered, washed, and recrystallized from ethanol to get **12** as a gray powder in a (46%) yield, mp >300 °C. IR (KBr) cm^{-1} ν_{max}: 3046 cm^{-1} (ν CH-Ar), 2989, 2945, 2921 cm^{-1} (ν CH aliphatic), 1744, 1684, 1667 cm^{-1} (ν 3C = O), 1619 cm^{-1} (ν C = N), 1553 cm^{-1} (C = C Ar). EI-MS: m/z ($C_{31}H_{22}N_6O_3S_2$) calcd = 590.68 [M^+].

4.2. Biological Activity. The supplemental data contained detailed descriptions of every in vitro and in vivo study.

4.3. In Silico Studies. *4.3.1. Molecular Docking Study.* The rationalization of biological observations has been aided by computational docking simulation. Using Auto Dock Vina 4.2 software, the fortunate thieno-thiazolo-quinazolines **4** and **5** were docked into the active pocket of *Staphylococcus aureus* DNA gyrase (PDB ID: 2XCT). Details can be found in the supporting file.

4.3.2. Quantum Chemical Calculation. Density Functional Theory (DFT) computations were performed using the B3LYP functional, a hybrid exchange-correlation functional that combines the gradient-corrected correlation functional of Lee, Yang, and Parr (LYP) with Becke's three-parameter exchange functional. By addressing integration concerns, this method has advantages over pure DFT techniques.

Gaussian 09 was used to fully optimize all molecular geometries at the B3LYP/6-311G++(d,p) level of theory. The energy gap (ΔE), global electrophilicity (ω), softness (σ), electronegativity (χ), hardness (η), and ionization potential (I) were then determined using frontier molecular orbital (FMO) analysis.

Using the optimized geometries, calculations were carried out at the B3LYP/6-31G level of theory in order to visualize the molecular electrostatic potential (MEP). The MEP maps reveal information about the molecules' electrophilic and nucleophilic areas.[72]

■ ASSOCIATED CONTENT

Supporting Information

The Supporting Information is available free of charge at https://pubs.acs.org/doi/10.1021/acsomega.4c11076.

Everything related to information about the devices and tools that were used; biological evaluation; enzyme assessment of DNA gyrase; molecular docking study; HOMO; LUMO of the assembled molecules; ^{1}H,^{13}C NMR, IR; mass spectra of the synthesized compounds (PDF)

■ AUTHOR INFORMATION

Corresponding Authors

Hagar S. El-Hema − *Basic Science Department (Chemistry), Thebes Higher Institute for Engineering, Thebes academy, Maadi 11434, Egypt*; orcid.org/0009-0000-3841-6122; Email: hagarsabry.23@yahoo.com

Adel A.-H. Abdel-Rahman − *Chemistry Department, Faculty of Science, Menoufia University, Shebin El-Kom 32511, Egypt*; Email: adelnassar63@yahoo.com

Authors

Sara. M. Soliman − *Chemistry Department, Faculty of Science, Benha University, Banha 13518, Egypt*

Wagdy El-Dougdoug − *Chemistry Department, Faculty of Science, Benha University, Banha 13518, Egypt*

Mohamed H. M. Ahmed − *Chemistry Department, Faculty of Science, Benha University, Banha 13518, Egypt*

Abdelmotaal Abdelmajeid − *Chemistry Department, Faculty of Science, Benha University, Banha 13518, Egypt*

Eman S. Nossier − *Pharmaceutical Medicinal Chemistry and Drug Design Department, Faculty of Pharmacy (Girls), Al-Azhar University, Cairo 11754, Egypt; The National Committee of Drugs, Academy of Scientific Research and Technology, Cairo 11516, Egypt*

Modather F. Hussein − *Chemistry Department, College of Science, Jouf University, Sakaka, Aljouf 72341, Saudi Arabia; Chemistry Department, Faculty of Science, Al-Azhar University, Assiut 71524, Egypt*

Ashtar A. Alrayes − *Chemistry Department, College of Science, Jouf University, Sakaka, Aljouf 72341, Saudi Arabia*

Mariam Hassan − *Department of Microbiology and Immunology, Faculty of Pharmacy Cairo University, Cairo 12411, Egypt; Department of Microbiology and Immunology, Faculty of Pharmacy, Galala University, New Galala City, Suez 991017, Egypt*

Noha A. Ahmed − *Department of Microbiology and Immunology, Faculty of Pharmacy Cairo University, Cairo 12411, Egypt*

Amr Sabry − *Department of pharmaceutical manufacturing, Faculty of Pharmacy, MUST University, Giza 3237101, Egypt*

Complete contact information is available at: https://pubs.acs.org/10.1021/acsomega.4c11076

https://doi.org/10.1021/acsomega.4c11076
ACS Omega 2025, 10, 9703−9717

Notes

The authors declare no competing financial interest.

■ ACKNOWLEDGMENTS

Thanks to Al-Jouf, Menoufia, and Benha University for participating in completing the research work.

■ REFERENCES

(1) Yang, Z.; Hu, Y.; Zhang, B.; Wang, Q.; Wang, Q.; Guo, Q. Preparation and antibacterial mechanism of copper-based silica nanocomposite materials. *Polyhedron.* **2024**, *255*, No. 116966.
(2) Zha, G.-F.; Preetham, H. D.; Rangappa, S.; et al. Benzimidazole analogues as efficient arsenals in war against methicillin-resistance staphylococcus aureus (MRSA) and its SAR studies. *Bioorg Chem.* **2021**, *115*, No. 105175.
(3) Verma, R.; Verma, S. K.; Rakesh, K. P.; Girish, Y. R.; Ashrafizadeh, M.; Sharath Kumar, K. S.; Rangappa, K. S. Pyrazole-based analogs as potential antibacterial agents against methicillin-resistance staphylococcus aureus (MRSA) and its SAR elucidation. *Eur. J. Med. Chem.* **2021**, *212*, No. 113134.
(4) Verma, S. K.; Verma, R.; Kumar, K. S. S.; Banjare, L.; Shaik, A. B.; Bhandare, R. R.; Rakesh, K. P.; Rangappa, K. S. A key review on oxadiazole analogs as potential methicillin-resistant *Staphylococcus aureus* (MRSA) activity: structure-activity relationship studies. *Eur. J. Med. Chem.* **2021**, *219*, No. 113442.
(5) Zha, G.-F.; Preetham, H. D.; Rangappa, S.; Sharath Kumar, K. S.; Girish, Y. R.; Rakesh, K. P.; Ashrafizadeh, M.; Zarrabi, A.; Rangappa, K. S. Benzimidazole analogues as efficient arsenals in war against methicillin-resistance *Staphylococcus aureus* (MRSA) and its SAR studies. *Bioorg. Chem.* **2021**, *115*, No. 105175.
(6) Fan, Z.; Cao, L.; He, Y.; Hu, J.; Di, Z.; Wu, Y.; Li, W.; Cao, Z. Ctriporin. a New antimethicillin-resistant *Staphylococcus aureus* peptide from the venom of the scorpion *Chaerilus tricostatus*. *Antimicrob. Agents Chemother.* **2011**, *55*, 5220−5229.
(7) Mai, T.; Toullec, J.; Van Wynsberge, S.; Besson, M.; Soulet, S.; Petek, S.; Aliotti, E.; Ekins, M.; Hall, K.; Erpenbeck, D.; Lecchini, D.; Beniddir, M. A.; Saulnier, D.; Debitus, C. Potential of Fascaplysin and Palauolide from *Fascaplysinopsis cf reticulata* to reduce the risk of bacterial infection in fish farming. *Fish. Aquat. Sci.* **2019**, *22*, 30.
(8) Wang, J.; Long, S.; Liu, Z.; Rakesh, K. P.; Verma, R.; Verma, S. K.; Sharath Kumar, K. S. Structure-activity relationship studies of thiazole agents with potential anti-methicillin-resistance *Staphylococcus aureus* (MRSA) activity. *Process Biochem.* **2023**, *132*, 13−29.
(9) Zhao, X.; Verma, R.; Sridhara, M. B.; Sharath Kumar, K. S. Fluorinated azoles as effective weapons in fight against methicillin-resistance *Staphylococcus aureus* (MRSA) and its SAR studies. *Bioorg. Chem.* **2024**, *143*, No. 106975.
(10) Bansal, S.; Bajaj, P.; Pandey, S.; Tandon, V. Topoisomerases: resistance versus sensitivity, how far we can go? *Med. Res. Rev.* **2017**, *37* (2), 404−438.
(11) Alamshany, Z. M.; Nossier, E. S. New Thiazole Derivatives Linked to Pyridine, Fused Pyridine, Pyrimidine and Thiazolopyrimidine Scaffolds with Potential Dual Anticancer and Antimicrobial Activities: Design, Synthesis and Docking Simulation. *J. Mol. Struct.* **2024**, *1316*, No. 138973.
(12) Xue, W.; Zuo, X.; Zhao, X.; Wang, X.; Zhang, X.; Xia, J.; Cheng, M.; Yang, H. Bioisosteric replacement strategy leads to novel DNA gyrase B inhibitors with improved potencies and properties. *Bioorg. Chem.* **2024**, *147*, No. 107314.
(13) Alsfouk, A. A.; Othman, I. M.; Anwar, M. M.; Alshareef, W. A.; Saleh, A.; Nossier, E. S. Synthesis and computational studies of new pyridine, pyrazole, pyran, and pyranopyrimidine-based derivatives of potential antimicrobial activity as DNA gyrase and topoisomerase IV inhibitors. *J. Mol. Struct.* **2025**, *1319*, No. 139528.
(14) Cheke, R. S.; Shinde, S. D.; Ambhore, J. P.; Chaudhari, S. R.; Bari, S. B. Quinazoline: An update on status against convulsions. *J. Mol. Struct.* **2022**, *1248*, No. 131384.
(15) Bhat, M.; Belagali, S. L.; Mamatha, S. V.; Sagar, B. K.; Sekhar, E. V. Importance of quinazoline and quinazolinone derivatives in medicinal chemistry. *Stud. Nat. Prod. Chem.* **2021**, *71*, 185−219.
(16) Singh, V. K.; Singh, S. K.; Gangwar, L. Synthesis, and antimicrobial activity of novel fused 4-(3H) quinazolinone derivatives. *Int. J. Sci. Res.* **2013**, *2*, 425−428.
(17) Guiles, J.; Sun, X.; Critchley, I. A.; Ochsner, U.; Tregay, M.; Stone, K.; et al. Quinazolin-2-ylamino-quinazolin-4-ols as novel non-nucleoside inhibitors of bacterial DNA polymerase III. *Bioorg. Med. Chem. Lett.* **2009**, *19*, 800−802.
(18) Sharma, P. C.; Kaur, G.; Pahwa, R.; Sharma, A.; Rajak, H. Quinazolinone Analogs as Potential Therapeutic Agents. *Curr. Med. Chem.* **2011**, *18* (27), 4786−4812.
(19) Jiang, S.; Zeng, Q.; Gettayacamin, M.; Tungtaeng, A.; Wannaying, S.; Lim, A.; et al. Antimalaria activities and therapeutic properties of febrifugine analogs. *Antimicrob. Agents Chemother.* **2005**, *49*, 1169−1176.
(20) Deetz, M. J.; Malerich, J. P.; Beatty, A. M.; Smith, B. D. One-step synthesis of 4(3H) quinazolinones. *Tetrahedron Lett.* **2001**, *42*, 1851−1854.
(21) Nagar, A. A.; Rathi, L. G.; Chugh, N.; Pise, V. J.; Bendale, A. Microwave assisted one pot synthesis of 2, 3-di-substituted quinazolin-4-(3H)-ones and their potential biological activity. *Der Pharm. Chem.* **2010**, *2*, 37−43.
(22) Mohi El-Deen, E. M.; Nossier, E. S.; Karam, E. A. New quinazolin-4(3H)-one derivatives incorporating hydrazone and pyrazole scaffolds as antimicrobial agents targeting DNA gyrase enzyme. *Sci. Pharm.* **2022**, *90* (3), 52.
(23) Raghavendra, N. M.; Thampi, P.; Gurubasavarajaswamy, P. M.; Sriram, D. Synthesis and antimicrobial activities of some novel substituted 2-imidazolyl−N-(4-oxo-quinazolin-3(4H)-yl) acetamides. *Chem. Pharm. Bull.* **2007**, *55*, 1615−1619.
(24) Du, C.; Yang, X.; Long, Y.; Lang, X.; Liu, L.; Xu, Y.; Wu, H.; Chu, Y.; Hu, X.; Deng, J.; Ji, Q. Design, synthesis and biological evaluation of novel spiro-quinazolinone derivatives as chitin synthase inhibitors and antifungal agents. *Eur. J. Med. Chem.* **2023**, *255*, No. 115388.
(25) Seifu, G. W.; Birhan, Y. S.; Beshay, B. Y.; et al. Synthesis, antimalarial, antileishmanial evaluation, and molecular docking study of some 3-aryl-2-styryl substituted-4(3H)-quinazolinone derivatives. *BMC Chem.* **2022**, *16*, 107.
(26) Xin, Y.; Xie, M.; Zou, L.-J.; Nie, K.; Wang, Y.-L. Synthesis and anticoccidial activity of 3-(2-(Benzofuran)-2-yl)-2-oxoethyl quinazolinone derivatives. *J. Chem. Res.* **2012**, *36* (3), 127−130.
(27) Al-Salahi, R.; Taie, H. A. A.; Bakheit, A. H.; et al. Antioxidant activities and molecular docking of 2-thioxobenzo[g]quinazoline derivatives. *Pharmacol. Rep.* **2019**, *71*, 695−700.
(28) Maarouf, A. R.; El-Bendary, E. R.; Goda, F. E. Synthesis and evaluation of some novel quinazolinone derivatives as diuretic agents. *Arch. Pharm. (Weinheim)* **2004**, *337* (10), 527−532.
(29) Hattori, K.; Kido, Y.; Yamamoto, H.; Ishida, J.; Iwashita, A.; Mihara, K. Rational design of conformationally restricted quinazolinone inhibitors of poly (ADP-ribose) polymerase. *Bioorg. Med. Chem. Lett.* **2007**, *17*, 5577−5581.
(30) Orvieto, F.; Branca, D.; Giomini, C.; Jones, P.; Koch, U.; Ontoria, J. M.; et al. Identification of substituted pyrazolo [1,5-a] quinazolin-5(4H)-one as potent poly (ADP-ribose) polymerase-1 (PARP-1) inhibitors. *Bioorg. Med. Chem. Lett.* **2009**, *19*, 4196−4200.
(31) Zeid, I. F.; Mohamed, N. A.; Khalifa, N. M.; Kassem, E. M.; Nossier, E. S.; Salman, A. A.; Mahmoud, K.; Al-Omar, M. A. PI3K Inhibitors of Novel Hydrazide Analogues Linked 2-Pyridinyl Quinazolone Scaffold as Anticancer Agents. *J. Chem.* **2019**, *2019* (1), No. 6321573.
(32) Abdel-Rahman, A. A. H.; El-Bayaa, M. N.; Sobhy, A.; El-Ganzoury, E. M.; Nossier, E. S.; Awad, H. M.; El-Sayed, W. A. Novel quinazolin-4-one based derivatives bearing 1, 2, 3-triazole and glycoside moieties as potential cytotoxic agents through dual EGFR and VEGFR-2 inhibitory activity. *Sci. Rep.* **2024**, *14* (1), 24980.

https://doi.org/10.1021/acsomega.4c11076
ACS Omega 2025, 10, 9703−9717

(33) Khalil, A. A.; Hamide, S. G. A.; Al-Obaid, A. M.; El-Subbagh, H. I. Substituted quinazolinones, Part 2. Synthesis and in vitro anticancer evaluation of new 2-substituted mercapto-3H-quinazolin analogs. *Arch. Pharm.* **2003**, *336*, 95−103.
(34) Zayed, M. F. Medicinal Chemistry of Quinazolines as Anticancer Agents Targeting Tyrosine Kinases. *Sci. Pharm.* **2023**, *91* (2), 18.
(35) Vijayakumar, K.; Ahamed, A. J.; Thiruneelakandan, G. Synthesis, antimicrobial, and anti-HIV activity of quinazoline-4(3H)-one derivatives. *J. Appl. Chem.* **2013**, *2013*, No. 387191.
(36) Jin, H.; Dan, H.-G.; Rao, G.-W. Research progress in quinazoline derivatives as multi-target tyrosine kinase inhibitors. *Heterocycl. Commun.* **2018**, *24* (1), 1−10.
(37) Al-Rashood, S. T.; Aboldahab, I. A.; Nagi, M. N.; Abouzeid, L. A.; Abdel-Aziz, A. A. M.; Abdel-hamid, S. G.; et al. Synthesis, dihydrofolate reductase inhibition, antitumor testing, and molecular modeling study of some new 4(3H)-quinazolinone analogs. *Bioorg. Med. Chem.* **2006**, *14*, 8608−8621.
(38) Khosropour, A. R.; Mohammadpoor-Baltork, I.; Ghorbankhani, H. Bi $(TFA)_3$-[nbp] $FeCl_4$: A new, efficient and reusable promoter system for the synthesis of 4(3H)-quinazolinone derivatives. *Tetrahedron Lett.* **2006**, *47*, 3561−3564.
(39) Liu, S.; Liu, F.; Yu, X.; Ding, G.; Xu, P.; Cao, J.; et al. The 3D-QSAR analysis of 4(3H)-quinazolinone derivatives with dithiocarbamate side chains on thymidylate synthase. *Bioorg. Med. Chem.* **2006**, *14*, 1425−1430.
(40) Raju, G. R.; Sai, K. B.; Resshma, V.; Sudarshini, N.; Sowmya, P. L.; Nalini, Y.; et al. Potential antimicrobial activities of quinazolinone derivatives. *J. Chem. Pharm. Res.* **2015**, *7*, 1279−1287.
(41) Patel, P. R.; Joshi, H.; Shah, U.; Bapna, M.; Patel, B. New Generation of Quinazolinone Derivatives as Potent Antimicrobial. *Agents Asian Pac. J. Health Sci.* **2021**, *8* (2), 128.
(42) Laddha, S. S.; Wadodkar, S. G.; Meghal, S. K. Studies on some biologically active substituted 4(3H)-quinazolinones. Part 1. Synthesis, characterization and anti-inflammatory, antimicrobial activity of 6,8-disubstituted 2-phenyl-3-[substituted-benzothiazol-2-yl]-4(3H)-quinazolinone. *Arkivoc* **2006**, *1*, 1−20.
(43) Al-Amiery, A. A.; Kadhum, A. A. H.; Shamel, M.; Satar, M.; Khalid, Y.; Mohamad, A. B. Antioxidant and antimicrobial activities of novel quinazolinones. *Med. Chem. Res.* **2014**, *23*, 236−242.
(44) Kumar, S.; Singh, B. R. An Overview of Mechanisms and Emergence of Antimicrobials Drug Resistance. *Emergence* **2013**, 10−14.
(45) Haque, M. Antibiotic use, antibiotic resistance, and antibiotic stewardship−A global public consequences. *Bangladesh J. Med. Sci.* **2019**, *18* (2), 169−170.
(46) Basha N, J.; Goudgaon, N. M. A comprehensive review on pyrimidine analogs-versatile scaffold with medicinal and biological potential. *J. Mol. Struct.* **2021**, *1246*, No. 131168.
(47) Kaur, R.; Kaur, P.; Sharma, S.; Singh, G.; Mehndiratta, S.; Bedi, P. M.; Nepali, K. Anticancer pyrimidines in diverse scaffolds: a review of patent literature. *Recent Pat. Anti-Cancer Drug Discovery* **2014**, *10* (1), 23−10.
(48) Manhas, N.; Singh, P.; Singh-Pillay, A.; Koorbanally, N. Synthesis, antibacterial screening and computational studies of quinazoline-4(3H)-one-triazole conjugates. *J. Mol. Struct.* **2023**, *1292*, No. 136108.
(49) Masri, A.; Anwar, A.; Khan, N. A.; Shahbaz, M. S.; Khan, K. M.; Shahabuddin, S.; Siddiqui, R. Antibacterial effects of quinazolin-4(3H)-one functionalized-conjugated silver nanoparticles. *Antibiotics* **2019**, *8* (4), 179.
(50) Ibrahim, A. O.; Hassan, A.; Mosallam, A. M.; Khodairy, A.; Rashdan, H. R.; Abdelmonsef, A. H. New quinazolin-2, 4-dione derivatives incorporating acylthiourea, pyrazole and/or oxazole moieties as antibacterial agents via DNA gyrase inhibition. *RSC Adv.* **2024**, *14* (24), 17158−17169.
(51) Gatadi, S.; Lakshmi, T. V.; Nanduri, S. 4(3H)-Quinazolinone derivatives: Promising antibacterial drug leads. *Eur. J. Med. Chem.* **2019**, *170*, 157−172.
(52) Hu, Y.; Hu, C.; Pan, G.; Yu, C.; Ansari, M. F.; Yadav Bheemanaboina, R. R.; Cheng, Y.; Zhou, C.; Zhang, J. Novel chalcone-conjugated, multi-flexible end-group coumarin thiazole hybrids as potential antibacterial repressors against methicillin-resistant *Staphylococcus aureus*. *Eur. J. Med. Chem.* **2021**, *222*, No. 113628.
(53) Wang, J.; Ansari, M. F.; Zhou, C. H. Identification of unique quinazolone thiazoles as novel structural scaffolds for potential gram-negative bacterial conquerors. *J. Med. Chem.* **2021**, *64*, 7630−7645.
(54) Katritzky, A. R.; Pozharskii, A. F. *Handbook of Heterocyclic Chemistry*. 2nd ed.; Pergamon Press: 1995.
(55) Mohi El-Deen, E. M.; Abd El-Meguid, E. A.; Karam, E. A.; Nossier, E. S.; Ahmed, M. F. Synthesis and biological evaluation of new pyridothienopyrimidine derivatives as antibacterial agents and *Escherichia coli* topoisomerase II inhibitors. *Antibiotics* **2020**, *9* (10), 695.
(56) Moustafa, G. O.; Shalaby, A.; Naglah, A. M.; Mounier, M. M.; El-Sayed, H.; Anwar, M. M.; Nossier, E. S. Synthesis, characterization, in vitro anticancer potentiality, and antimicrobial activities of novel peptide−glycyrrhetinic-acid-based derivatives. *Molecules* **2021**, *26* (15), 4573.
(57) Othman, I. M.; Alamshany, Z. M.; Tashkandi, N. Y.; Nossier, E. S.; Anwar, M. M.; Radwan, H. A. Chemical synthesis and molecular docking study of new thiazole, thiophene, and thieno [2, 3-d] pyrimidine derivatives as potential antiproliferative and antimicrobial agents. *J. Mol. Struct.* **2022**, *1270*, No. 133926.
(58) El-Serwy, W. S.; Mohamed, H. S.; El-Serwy, W. S.; Mohamed, N. A.; Kassem, E. M.; Nossier, E. S.; Shalaby, A. S. G. Molecular docking study of newly synthesized thiopyrimidines as antimicrobial agents targeting DNA gyrase enzyme. *J. Heterocyclic Chem.* **2019**, *56* (7), 2027−2035.
(59) Ali, N. B.; El-Shiekh, R. A.; Ashour, R. M.; El-Gayed, S. H.; Abdel-Sattar, E.; Hassan, M. In vitro and in vivo antibiofilm activity of red onion scales: An agro-food waste. *Molecules.* **2023**, *28* (1), 355.
(60) Albash, R.; Abdellatif, M. M.; Hassan, M.; Badawi, N. M. Tailoring terpesomes and leciplex for the effective ocular conveyance of moxifloxacin hydrochloride (Comparative assessment): in-vitro, ex-vivo, and in-vivo evaluation. *Int. J. Nanomed.* **2021**, 5247−5263.
(61) Ismail, M. M.; Hassan, M.; Moawad, S. S.; Okba, M. M.; Ashour, R. M.; Fayek, N. M.; Saber, F. R. Exploring the antivirulence activity of pulverulentone A, a phloroglucinol-derivative from *Callistemon citrinus* leaf extract, against multi-drug resistant *Pseudomonas aeruginosa*. *Antibiotics.* **2021**, *10* (8), 907.
(62) El-Naggar, M. M.; El-Nabarawi, M. A.; Teaima, M. H.; Hassan, M.; Hamed, M. I. A.; Elrashedy, A. A.; Albash, R. Integration of terpesomes loaded Levocetrizine dihydrochloride gel as a repurposed cure for Methicillin-Resistant *Staphylococcus aureus* (MRSA)-Induced skin infection; D-optimal optimization, ex-vivo, in-silico, and in-vivo studies. *Int. J. Pharm.* **2023**, *633*, No. 122621.
(63) El-Shiekh, R. A.; Hassan, M.; Hashem, R. A.; Abdel-Sattar, E. Bioguided isolation of antibiofilm and antibacterial pregnane glycosides from *Caralluma quadrangula*: Disarming multidrug-resistant pathogens. *Antibiotics.* **2021**, *10* (7), 811.
(64) Hussein, M. E.; Mohamed, O. G.; El-Fishawy, A. M.; El-Askary, H. I.; El-Senousy, A. S.; El-Beih, A. A.; Nossier, E. S.; Naglah, A. M.; Almehizia, A. A.; Tripathi, A.; Hamed, A. A. Identification of antibacterial metabolites from endophytic fungus *Aspergillus fumigatus*, isolated from *Albizia lucidior* leaves (Fabaceae), utilizing metabolomic and molecular docking techniques. *Molecules.* **2022**, *27* (3), 1117.
(65) Kassem, A. F.; Younis, A.; Nossier, E. S.; Awad, H. M.; El-Sayed, W. A. Pyridine-Based Glycosides Bearing 1, 2, 4-Triazole and Their 1, 3, 4-Oxadiazole Analogues as Potential EGFR and CDK-2 Inhibitors: Design, Synthesis, Antiproliferative Activity and In Silico Studies. *J. Mol. Struct.* **2024**, *1313*, No. 138741.
(66) Batran, R. Z.; Ahmed, E. Y.; Nossier, E. S.; Awad, H. M.; Abdel Latif, N. A. Anticancer activity of new triazolopyrimidine linked coumarin and quinolone hybrids: Synthesis, molecular modeling,

https://doi.org/10.1021/acsomega.4c11076
ACS Omega 2025, 10, 9703−9717

TrkA, PI3K/AKT and EGFR inhibition. *J. Mol. Struct.* **2024**, *1305*, No. 137790.
(67) Sheta, Y. S.; Sarg, M. T.; Abdulrahman, F. G.; Nossier, E. S.; Husseiny, E. M. Novel imidazolone derivatives as potential dual inhibitors of checkpoint kinases 1 and 2: Design, synthesis, cytotoxicity evaluation, and mechanistic insights. *Bioorg. Chem.* **2024**, *149*, No. 107471.
(68) Dawood, D. H.; Sayed, M. M.; Tohamy, S. T.; Nossier, E. S. New Thiophenyl-pyrazolyl-thiazole Hybrids as DHFR Inhibitors: Design, Synthesis, Antimicrobial Evaluation, Molecular Modeling, and Biodistribution Studies. *ACS Omega.* **2023**, *8* (42), 39250−39268.
(69) Alamshany, Z. M.; Algamdi, E. M.; Othman, I. M.; Anwar, M. M.; Nossier, E. S. New pyrazolopyridine and pyrazolothiazole-based compounds as anti-proliferative agents targeting c-Met kinase inhibition: Design, synthesis, biological evaluation, and computational studies. *RSC Adv.* **2023**, *13* (19), 12889−12905.
(70) Cheng, F.; Yu, Y.; Shen, J.; Yang, L.; Li, W.; Liu, G.; Lee, P. W.; Tang, Y. Classification of cytochrome P450 inhibitors and non-inhibitors using combined classifiers. *J. Chem. Inf. Model.* **2011**, *51* (5), 996−1011.
(71) Williams, J. A.; Hyland, R.; Jones, B. C.; Smith, D. A.; Hurst, S.; Goosen, T. C.; Peterkin, V.; Koup, J. R.; Ball, S. E. Drug-drug interactions for UDP-glucuronosyltransferase substrates: A pharmacokinetic explanation for typically observed low exposure (AUCi/AUC) ratios. *Drug Metab. Dispos.* **2004**, *32* (11), 1201−1208.
(72) Wu, S.; Zhang, W.; Qi, L.; Ren, Y.; Ma, H. Investigation on 4-amino-5-substituent-1,2,4-triazole-3-thione Schiff bases as antifungal drug by characterization (spectroscopic, XRD), biological activities, molecular docking studies and electrostatic potential (ESP). *J. Mol. Struct.* **2019**, *1197*, 171−182.

https://doi.org/10.1021/acsomega.4c11076
ACS Omega 2025, 10, 9703−9717